CPH_TechnicalMemo_Coastal_Final_Draft

Prepared by: Bonnie C. Ludka, Jeffrey K. Anderson, Seth Casanova & Umesh P. A. Pillai

Summary of work

This report assesses the shoreline geomorphology and coastal flooding vulnerability of the region surrounding Wigi (Humboldt Bay), focusing on the low-lying Eureka/Arcata Corridor of Highway 101, a crucial transportation route in Humboldt County. Photos and georeferenced historical maps are used to analyze shoreline conditions and evolution. A hydrodynamic model, wave model, and empirical formulations are used to evaluate coastal flooding vulnerability. Building on the EFDC (Environmental Fluid Dynamics Code) hydrodynamic model developed by NHE (2015), we estimate reference water levels (tide, non-tidal residual, and local wind set up) based on 74-years of tide gauge and wind observations. Reference level extreme recurrence intervals are estimated using the Generalized Pareto Distribution- Peaks Over Threshold method. The 2-D SWAN (Simulating WAves Nearshore) model is used to simulate the generation, propagation and dissipation of waves across the bay. Look-up tables of bulk wave parameters are generated numerically for locations near the structure toe along the corridor for a range of realistic forcing conditions. Time series of wave conditions are generated by querying the look-up table for the simulated reference water levels and observed wind conditions. Wave runup, and overtopping and overflow discharge are estimated empirically following EurOTop (2018), using the modeled bulk wave parameters and the shoreline structure's geometric characteristics (e.g. slope, height, crest width). The model framework is applied for a range of sea level futures that account for local vertical land motion.

1. Coastal setting

Wigi (Humboldt Bay) is located approximately 260 miles (418 km) north of San Francisco, California, and is the second largest natural bay in California (Costa and Glatzel, 2002). Wigi is situated within the 42 mile (67 km) long Eureka littoral cell (ELC) which is bounded by Trinidad Head in the north and False Cape in the south. The ELC has an approximate 4,520 mi^2 (11,700 km^2) contributing watershed, and the two largest rivers, the Wiya't and Baduwa't (renamed by colonizers to the Eel and Mad River, respectively) discharge directly into the ELC (Figure 1.1). In comparison, Wigi's watershed is relatively small at 223 mi^2 (578 km^2). Wigi consists of three basins, Arcata Bay (or North Bay), Entrance Bay and South Bay (Figure 1.2). The North Bay Channel runs from the Entrance Bay to North Bay where it splits into multiple channels. The transition between South Bay to Entrance Bay is delineated by a constriction between the South Bay spit and King Salmon.

Figure 1.1: The Eureka littoral cell.

The four largest streams entering Wigi are Jacoby Creek and Freshwater Creek that discharge into North Bay, Elk River that discharges into the northern end of Entrance Bay, and Salmon Creek that discharges into South Bay. Due to the small watershed size and low freshwater flows, Wigi

is tidally dominated and consists of well-mixed marine water. Seasonal estuarine conditions occur in the sub-estuary regions of the bay tributaries (Costa and Glatzel, 2002).

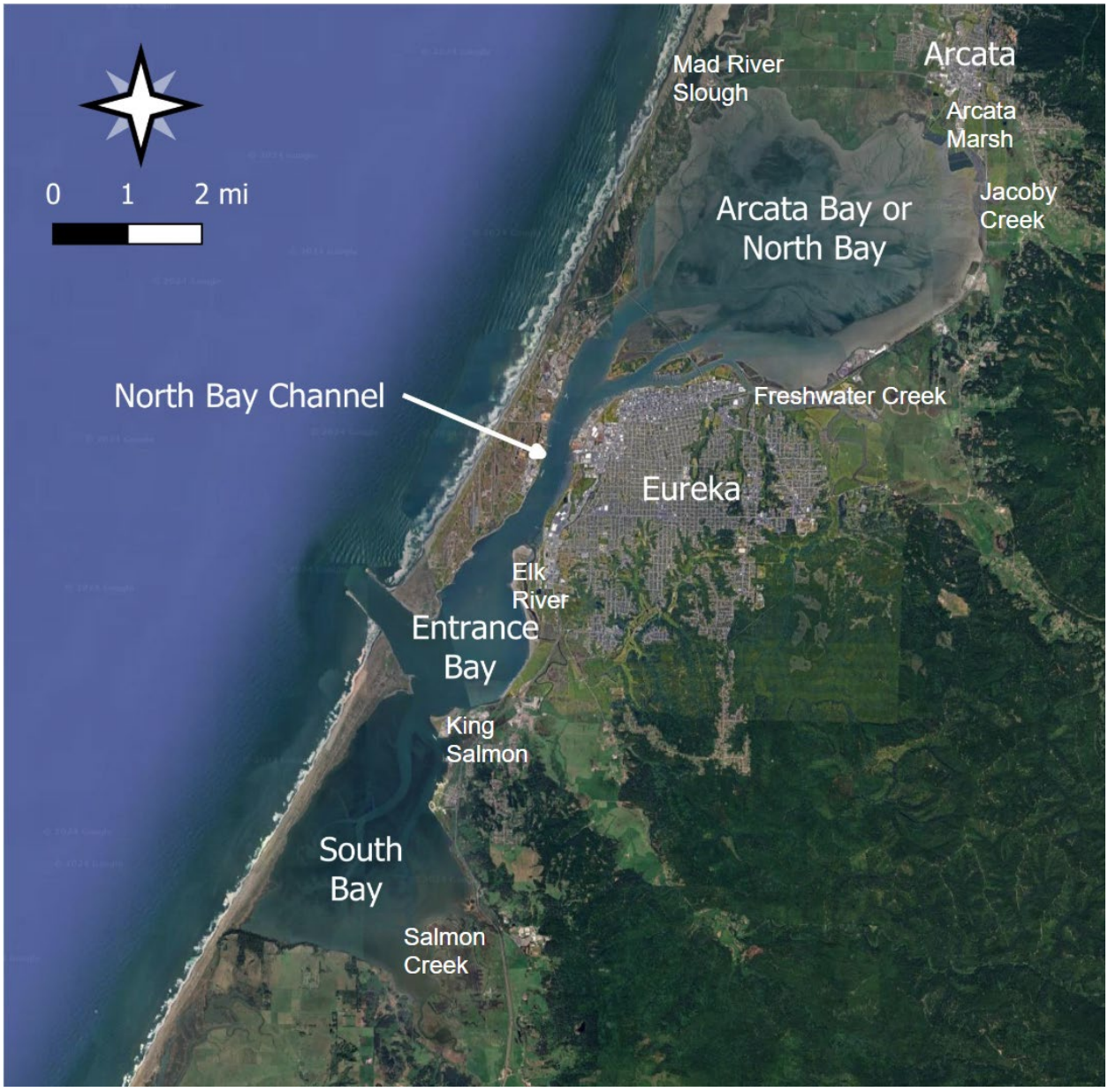

Figure 1.2: Wigi, with its basins and major surrounding cities and tributaries labeled.

Wigi's tides are mixed semidiurnal, with tidal amplification and phase that lags with distance from the entrance (Costa and Glatzel, 2002; NHE, 2015). The tidal prism is approximately 9.63 to 9.91 x 10^7 cubic meters during a spring tide range and about 70% less over a mean tide range (Costa and Glatzel, 2002). Arcata Bay contributes approximately 50% of the tidal prism whereas South

Bay contributes approximately 30%. Arcata Bay has a mean tide range of approximately 4.8 feet, diurnal range of 6.7 feet, and a maximum range of about 11 feet during spring tides.

Daily low tides expose extensive mudflats, and high diurnal tides inundate salt marshes. Salt marsh ecosystems in Wigi establish at elevations approximately from mean high water (MHW) to over mean higher high water (MHHW) and are periodically inundated by extreme high tides. Along the Eureka/Arcata corridor, salt marsh primarily exists in the southern and northern segments (Sections A and C in Figure 1.3). Wigi has a water surface area of approximately 25 mi^2 (65 km^2) at high tide, and 8 mi^2 (21 km^2) at low tide. Approximately 70% of the bay is exposed tidal mudflat at low tide, where most of the mudflats are located in the shallower North and South Bays (Costa and Glatzel, 2002). The upper sub-tidal mudflats support an abundance of eelgrass and are incised by subtidal channels.

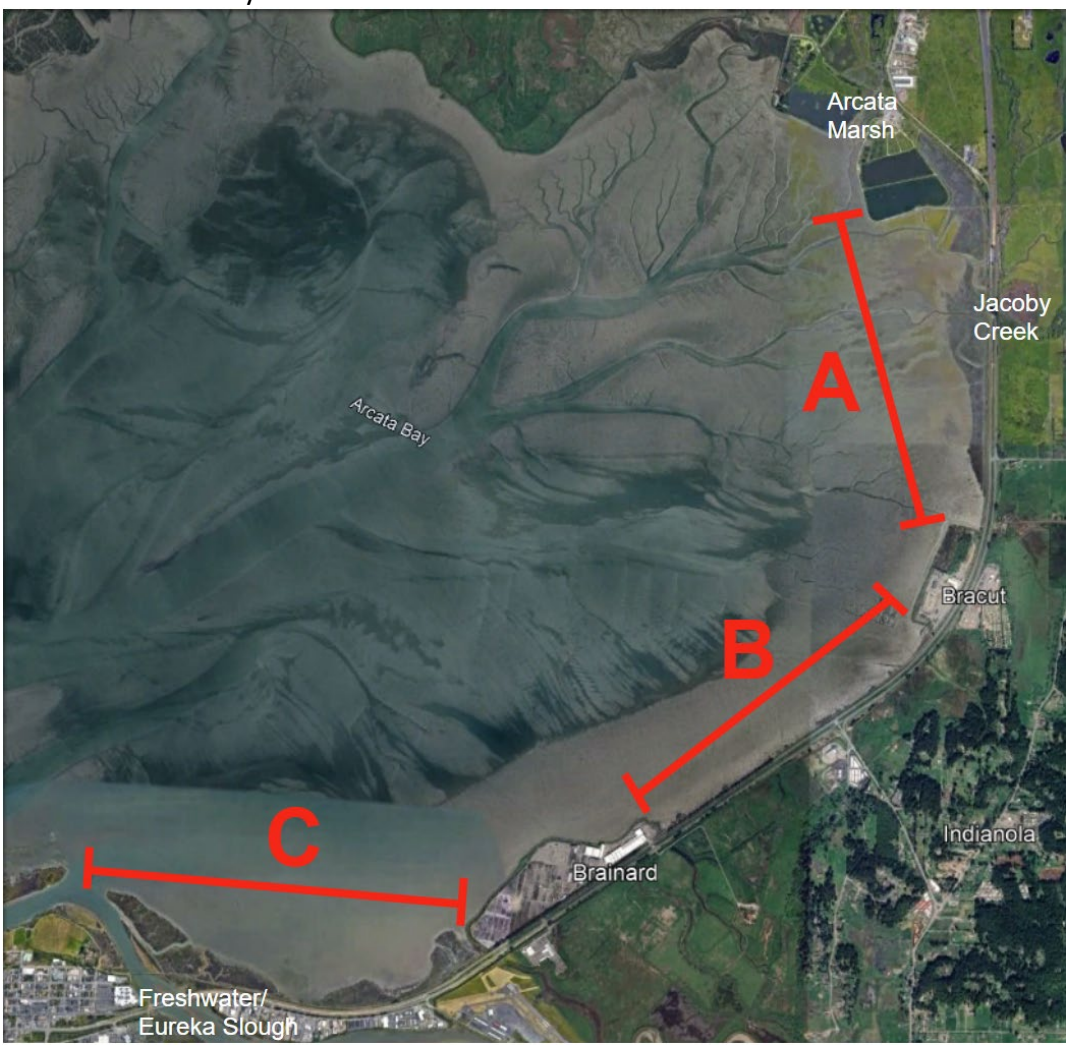

Figure 1.3: Shoreline segments adjacent to the Eureka/Arcata corridor.

Sediments in Wigi include silt, clays, and coarse material (e.g., sand, shell fragments) and their spatial patterns are associated with bay morphology, hydrodynamics and wave exposure (Thompson, 1971). The bottoms of tidal channels are covered by gravelly and shelly sand that becomes finer and muddier with increasing distance from the inlet. Clayey silt dominates the tidal flats, and organic silty clay or clayey peat is found in salt marshes (GHD et al., 2022).

The outer coast wave climate is dominated by large frequent swells (Wheatcroft and Borgeld, 2000; Costa and Glatzel, 2002; George and Hill, 2008) which enter Wigi via the jettied channel into Entrance Bay. The Eureka/Arcata corridor is located along the coast of eastern Arcata Bay which is sheltered from the large swell waves that frequent the Entrance Bay. However, local strong wind events can generate short-period waves with significant wave heights that are a couple feet tall along the corridor shoreline (FEMA 2014 and ESA 2018).

Flume experiments using sediments collected from the mudflats in Arcata Bay estimate the critical shear stress for incipient sediment motion (GHD et al., 2022). Numerical experiments show that tidal-induced currents alone can mobilize sediment in the mudflats that are exposed at low tide, but in general current-induced sediment motion is low in the intertidal region (GHD et al., 2022). Wave-induced stresses mobilize sediment throughout the intertidal zone in the model, demonstrating that wind-waves are likely the dominant initiator for mudflat sediment redistribution, even in the sheltered bays.

Wigi's sediments are predominantly from fluvial runoff and marine input (Barnhart, 1992). Thompson (1971) estimated a yearly input of 540,000 to 670,000 m^3 from marine sediments and 90,000 m^3 from fluvial tributaries to the Bay. Most of the oceanic sediment is derived indirectly from fluvial sources within the Eureka Littoral cell, predominantly from the Eel River. The United States Army Corps of Engineers (USACE) performs maintenance dredging of the federal navigation channels and has reported removal rates of approximately 690,000 m^3/year between 1975 and 2016, consistent with the estimated total sediment input volume rate. The total dredged volume is approximately 10% fine sediment, with 90% sand size and larger. Starting in 1990, dredged material was placed offshore approximately 3.5 mi from the channel entrance (USACE, 2017).

Wigi has and will continue to evolve with sea level rise (SLR). Wigi was previously a river valley when sea level was 100-200 meters lower and then drowned as seas rose with the end of the last ice age (~15,000 to 20,000 years ago; Barnhart et al., 1992). Thompson (1971) suggested that the presence of extensive tidal flats and salt marsh imply former high rates of accretion and bay infill. Accretion rates measured in Jacoby Creek marsh appear lower than relative SLR (Curtis et al., 2019) while historical accretion rates are estimated to have kept pace or slightly outpaced relative SLR (Thompson 1971; Brown, 2019). While a sediment budget has not been completed

for Wigi, climate change models predict an increase in suspended sediment delivery to the Eureka Littoral Cell and the Bay, which could partially offset impacts from sea level rise and subsidence (Curtis, 2021).

1.1 Land use

The Wiyot people are the indigenous peoples of Wigi and the surrounding region. Before colonization Wiyot people lived in villages along the bay and surrounding waterways, and traveled between these villages by canoe. Wiyot people actively managed the area's natural resources and they continue to be stewards of the land today. The Gold Rush and the logging boom brought white settlers to the region, who depleted the region of natural resources, spread disease, and displaced, enslaved, and massacred the Wiyot people (Wiyot Tribe, 2024).

By constructing levees and drainage structures, colonizers converted tidelands to agricultural land (Rohde, 2020)**. Tidewaters were also blocked by the construction of elevated railroad and road prisms. This infrastructure has reduced salt marsh habitat, has altered the shoreline, and once constructed, often fixes the shoreline in place** (Figure 1.1.1; Laird et al., 2013, Richmond et al., 2023).

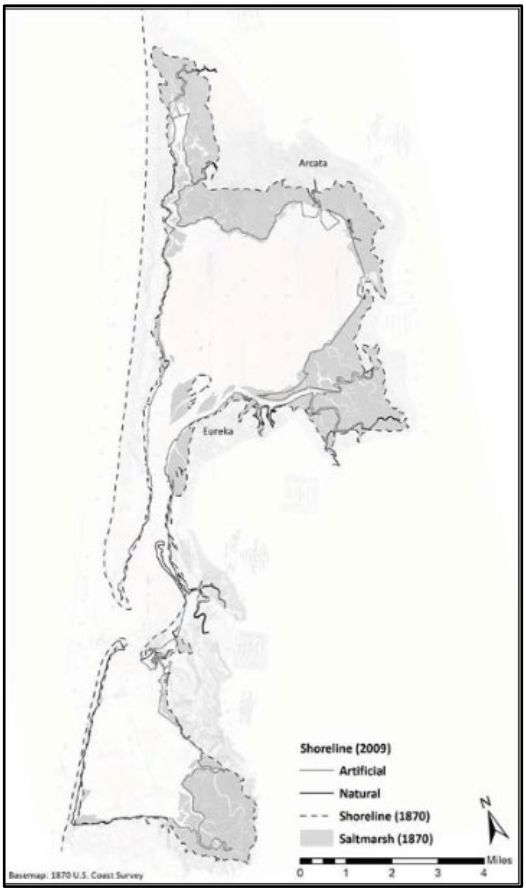

Figure 1.1.1: Wigi's 1870 Shoreline compared to the 2009 Shoreline. Figure by Jay Patton from Richmond et al. (2023), based on Laird et al. (2013)

Using ArcGIS, 32 historical maps from the United States Coast and Geodetic Survey (USCGS) United States Department of Commerce (USDC), United States Army Corps of Engineers (USACE), United States Department of Agriculture (USDA), and others were georeferenced using visual tie points to a common basemap for time periods between 1884 and 2010. A selection of these maps showing significant shifts in coastal features, land use and shape are presented in Figures 1.1.2-7. Additional maps that encompass or include subsets of this region can be found in GHD (2021), GHD et al. (2022) and others. Often maps with a particular publication date were created using survey data from an older date, so care must be taken to note both.

Rhode (2020) documented many of the land use changes in Wigi that occurred after settler colonists arrived. Between 1854-1890 a canal connecting Baduwa't (Mad) River to Arcata Bay was constructed (Mad River Slough) and in 1881 the Eureka-Arcata navigation channel was dredged. In 1889 the ocean entrance to Wigi was modified and armored with rock. A levee between Butcher Slough (now within Arcata Marsh, Figure 1.3) and Jacoby Creek mouth was constructed in 1892. Between 1895-1898 the former salt marsh edge was leveed from what is now Brainard and Bracut (Figure 1.3) and Freshwater/Eureka Slough creating approximately 1,000 acres of diked former tideland (Figure 1.1.3). Two rail prisms (E&KRR and C&N's NWP) were constructed in 1900 (C&N's NWP tracks were laid in 1900, while the E&KRR tracks were never laid). The construction of the Eureka/Arcata corridor in the 1920's created an additional tidal barrier, seen in the maps as the reduction of marsh area around Freshwater Slough (Figures 1.1.4-5). In the 1950's the Bracut peninsula was expanded and an additional 2 lanes were added to the highway (Figure 1.1.6). The final map (Figure 1.1.7) is representative of modern day conditions.

Figure 1.1.2: This UCSGS map (published in 1984) uses 1870 topography. It shows extensive salt marsh in western Arcata Bay.

Figure 1.1.3: This 1916 USACE map (publication date and survey data both collected in 1916) was one of the first primary sources known to remove marsh classification around Brainard, Indianola, and Bayside. C&N's NWP railroad can be seen running from Eureka to Arcata.

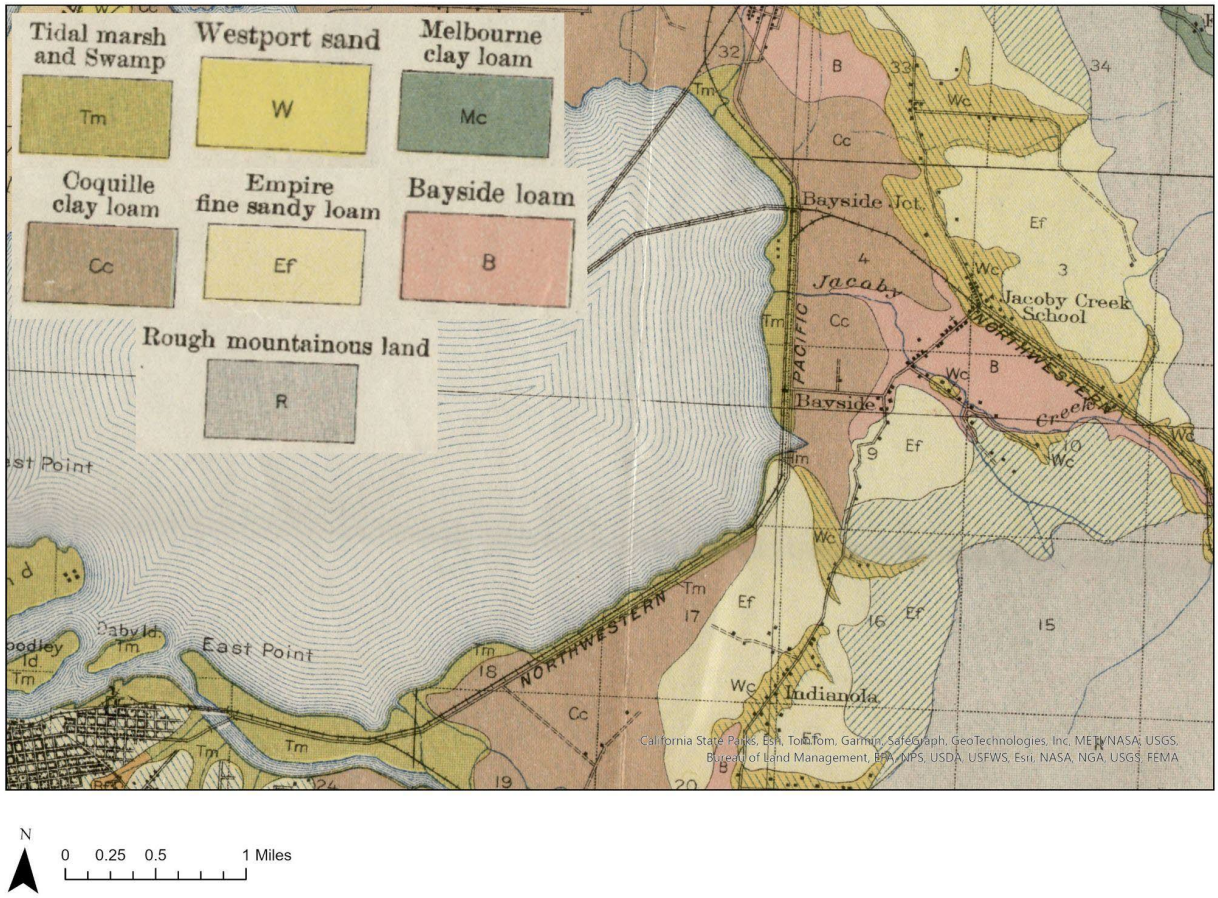

Figure 1.1.4: Land classifications in this 1921 USDA map provide more context for land usage and subdivisions along the coast before construction of the 101 freeway. Note land near Freshwater Slough is classified as tidal marsh.

Figure 1.1.5: This State of California map with topographic survey data and features drawn for 1933 displays the Redwood Highway, now the 101 freeway (constructed 1918-1925). The area between the highway and Freshwater Slough (known as Eureka Slough closer to Eureka), is no longer classified as marsh. The abandoned and eroding E&KRR *rail prism between Brainard and Bracut can be seen in segmented pieces along the shoreline.*

Figure 1.1.6: This 1958 aerial imagery from the Humboldt Bay / Eel River Delta Historic Atlas displays the early construction phases of Bracut and Arcata Marsh. The levees around Bracut have been constructed in the image, but have not been completely infilled. Similarly, one of the treatment ponds for the Arcata March has been walled. The imagery also shows the current shape of the 101 freeway that cuts through the city of Arcata instead of following the shoreline, modified when the highway was expanded from a 2-lane to a 4-lane highway in 1955.

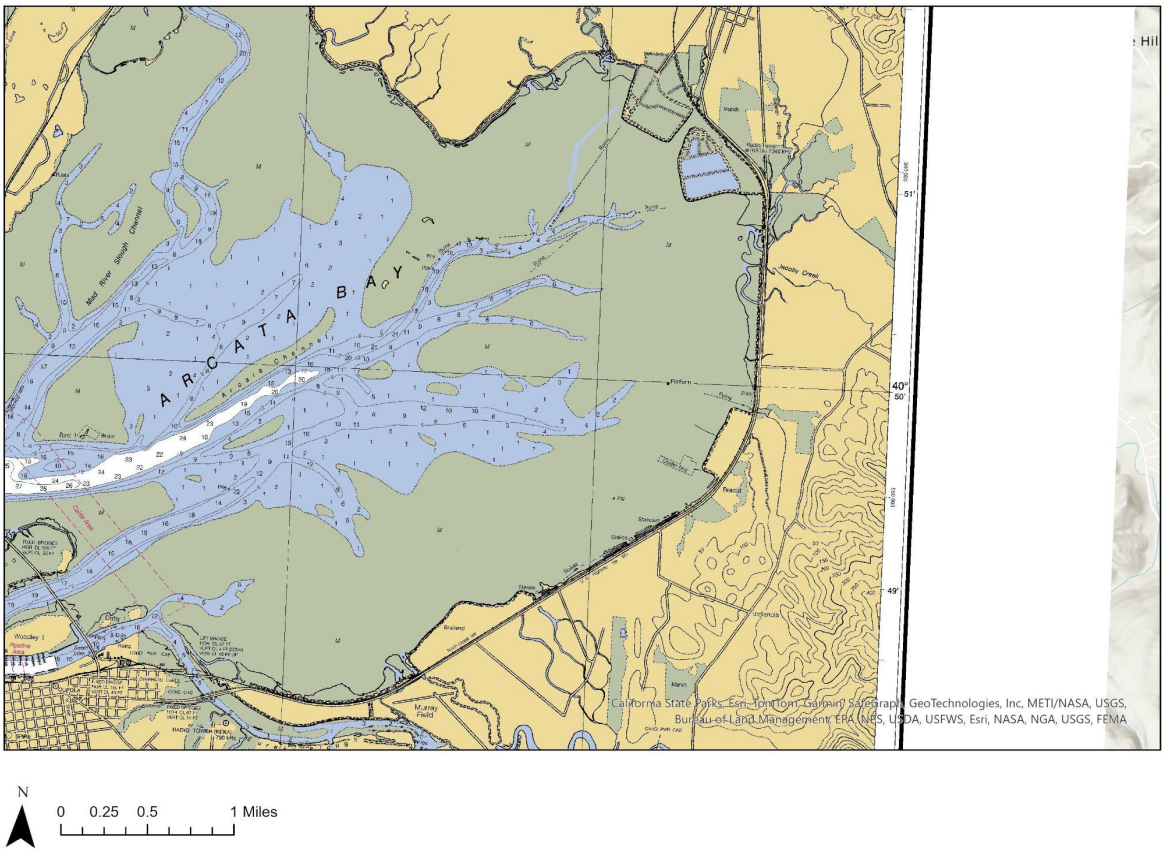

Figure 1.1.7: The 2010 US Coast and Geodetic Survey map shows Bracut expansion (completed 1960) and the completed Arcata Marsh Wastewater Treatment Plant (constructed in 1981).

1.2 Existing shoreline

The existing shoreline is documented using photographs taken along the corridor, where the photos are arranged along three shoreline segments (Figure 1.3). Segments A (Figure 1.2.1) and C (Figure 1.2.3) have larger areas of salt marsh along the shoreline than segment B (Figure 1.2.2). By analyzing maps similar to those shown above, GHD et al. (2022) found that shoreline segment B has experienced greater salt marsh erosion than shoreline segments A and C. They found that marsh edge positions in segment A and C are fairly static, suggesting an ongoing process of erosive scarping, followed by accretion and revegetation. The Bracut and Brainard peninsula shorelines are primarily riprap (not shown). Extensive mudflats and some pocket beaches of sand and cobble (formed by erosion of the historical railroad prism) are exposed at lower water levels (not shown). Additional photos can be found in Laird et al. (2013), GHD (2018), GHD et al. (2022) and others.

Figure 1.2.1: Photos along Segment A (Figure 1.3) of the corridor shoreline with northernmost photos at the top and southernmost photos at the bottom. This segment primarily consists of salt marsh interspersed with tributaries, with a smaller segment of riprap in the south (bottom). The bay trail is completed here, with bridges over the tributaries (top right)

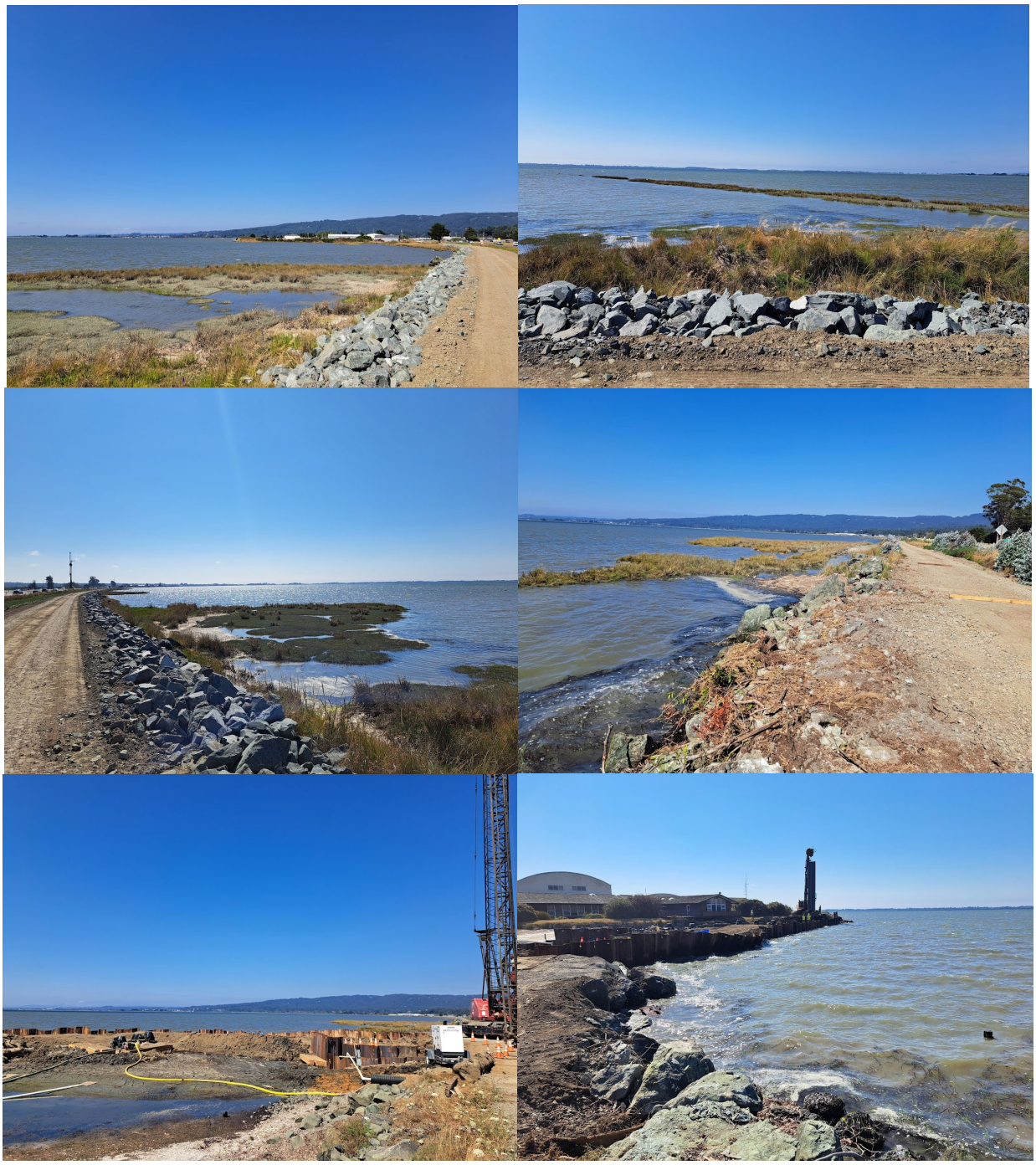

Figure 1.2.2: Photos along Segment B (Figure 1.3) of the corridor shoreline with northernmost photos at the top and southernmost photos at the bottom. This segment is primarily riprap, with a remnant earthen "peninsula" levee (top right, constructed in 1960 as part of an abandoned attempt to expand Bracut; Rohde 2020), and small swaths of salt marsh (center). The bay trail is under construction and abuts the shoreline.

Figure 1.2.3: Photos along Segment C (Figure 1.3) of the corridor shoreline with easternmost photos at the top and westernmost photos at the bottom. This segment is primarily fronted by salt marsh with the Freshwater Slough Channel and Bridge in the west (bottom). The bay trail is under construction (center-left).

1.3 Bathymetry and topography

Project area topography and bathymetry was defined by the 2020 USGS Coastal National Elevation Database (CoNED) 1-meter topobathymetric digital elevation model (TBDEM) for the Northern California Coast (2020 USGS CoNED DEM). The 2020 USGS CoNED DEM (or Project DEM) consists of multiple topographic and bathymetric data sets ranging in dates from approximately 1986 to 2019 that have been aligned vertically and horizontally to a common reference system (OCM Partners, 2024). Figure 1.3.1 shows the topography and bathymetry along the corridor in eastern Arcata Bay.

According to the online metadata information (OCM Partners, 2024), it appears the topographic data surrounding Humboldt Bay relied on the City of Eureka 2019 Humboldt Bay LiDAR (24 September 2019 acquisition date). For this assessment, it was assumed the City of Eureka 2019 LiDAR represents ground elevations in 2019 at the time of the acquisition and has not been adjusted for vertical land motion either before or after the acquisition date. This distinction is important when comparing ground elevations to observed or modeled water surface elevations, and when considering future sea-level change.

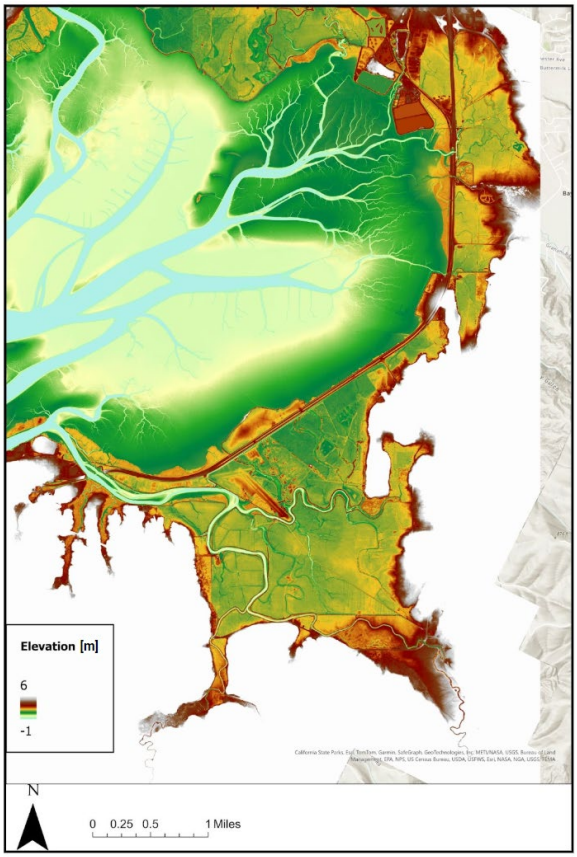

Figure 1.3.1: 2020 USGS Coastal National Elevation Database (CoNED) 1-meter topobathymetric digital elevation model (TBDEM). Elevations are in meters relative to NAVD88.

1.4 Extraction Points

Throughout this report we use "extraction points" that are representative locations along the Eureka/Arcata corridor to showcase results (Figure 1.4.1). Points 1 and 2 are in Section A, Points 3 and 4 are in Section B, and Point 5 is in Section C (Figure 1.3).

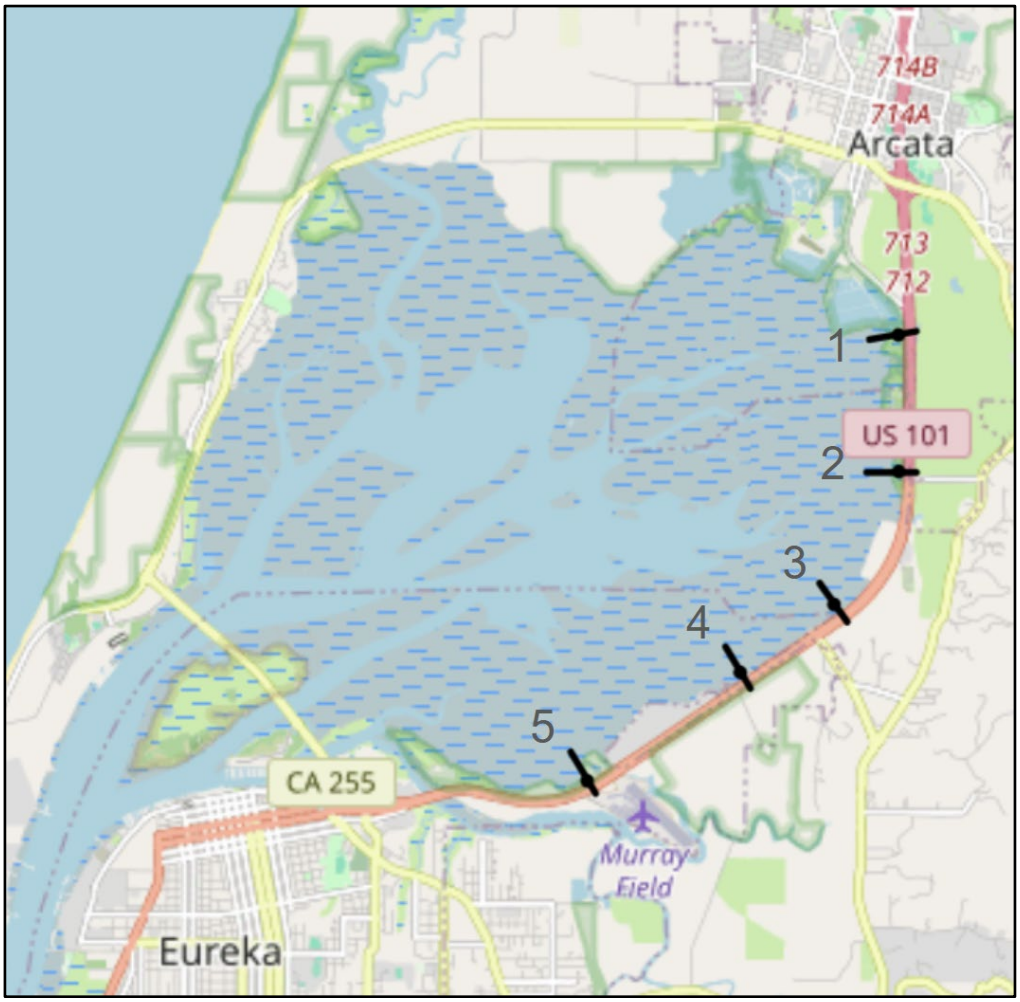

Figure 1.4.1: Extraction Points (black circles). Black lines show the orientation of the shoreline protective structure at each location and represent the profile transects shown in Figure 1.4.7

The extraction points (Table 1.4.1) are located seaward of the toe of the structure to avoid any model edge effects. The protective structure landward of the extraction point was characterized at each location (Figures 1.4.2-8, Table 1.4.2).

Table 1.4.1: Location, elevation, and substrate type for extraction points.

Point	Latitude (°)	Longitude (°)	Elevation [ft, NAVD88]	Substrate Type
1	40.84853830	-124.0831946	6.6	Salt Marsh
2	40.83571592	-124.0831467	6.8	Salt Marsh
3	40.82324657	-124.0911922	3.3	Mud Flat
4	40.81686477	-124.1028397	3.6	Mud Flat
5	40.80667658	-124.1218314	6.3	Salt Marsh

Figure 1.4.2: Extraction Point 1. [Top]: Looking out on an extensive salt marsh from the location of the extraction point. [Bottom Left]: The location of the actual extraction point on the salt marsh, looking towards the highway. [Bottom Right]: Near the base of the shoreline protection structure which is vegetated mud and cobble from the old railroad prism (ORP). There is a slough channel fronting the old railroad prism.

Figure 1.4.3: Extraction Point 2. [Top]: The location of the actual extraction point on the salt marsh, looking towards the highway. [Bottom Left]: The edge of the salt marsh, looking towards the bay. [Bottom Right]: Near the base of the shoreline protection structure, which consists of vegetated cobble and mud from the old railroad prism (ORP). There is a narrow slough channel fronting the old railroad prism.

Figure 1.4.4: Extraction Point 3. The location of the actual extraction point is on the mud flat. [Left]: Looking north from the top of the protective shoreline structure which is characterized as Rocky Shore Protection (RSP, or "riprap"). (The seal was rescued shortly after we reported its sickly presence.) [Right]: Looking south from the top of the protective shoreline structure. (If you look closely in the lower right you might be able to see where Bonnie almost lost her boot attempting to access the extraction point in the mud.)

Figure 1.4.5: Extraction Point 4. The location of the actual extraction point is on the mud flat. [Left]: Looking north from the top of the protective shoreline structure which is characterized as Rocky Shore Protection (RSP, or "riprap"). [Right]: Looking south from the top of the protective shoreline structure.

Figure 1.4.6: Extraction Point 5. [Top]: Looking towards the highway from the location of the extraction point. [Bottom Left]: Looking west from the edge of the salt marsh. [Bottom Right]: Near the base of the shoreline protection structure which is vegetated mud and cobble from the old railroad prism (ORP).

The differences in the salt marsh extent fronting the shoreline structure at each point can be seen in Figure 1.4.7, while the differences in the heights and shapes of the protective shoreline structure are shown in Figure 1.4.8 and Table 1.4.2. **After completion of the Bay Trail, Points 3 and 4 will have the tallest protective shoreline structure. However, note that the highway elevation is lowest at Points 3 and 4, so these locations could still be the most vulnerable if water gets in elsewhere** (Figure 1.4.9).

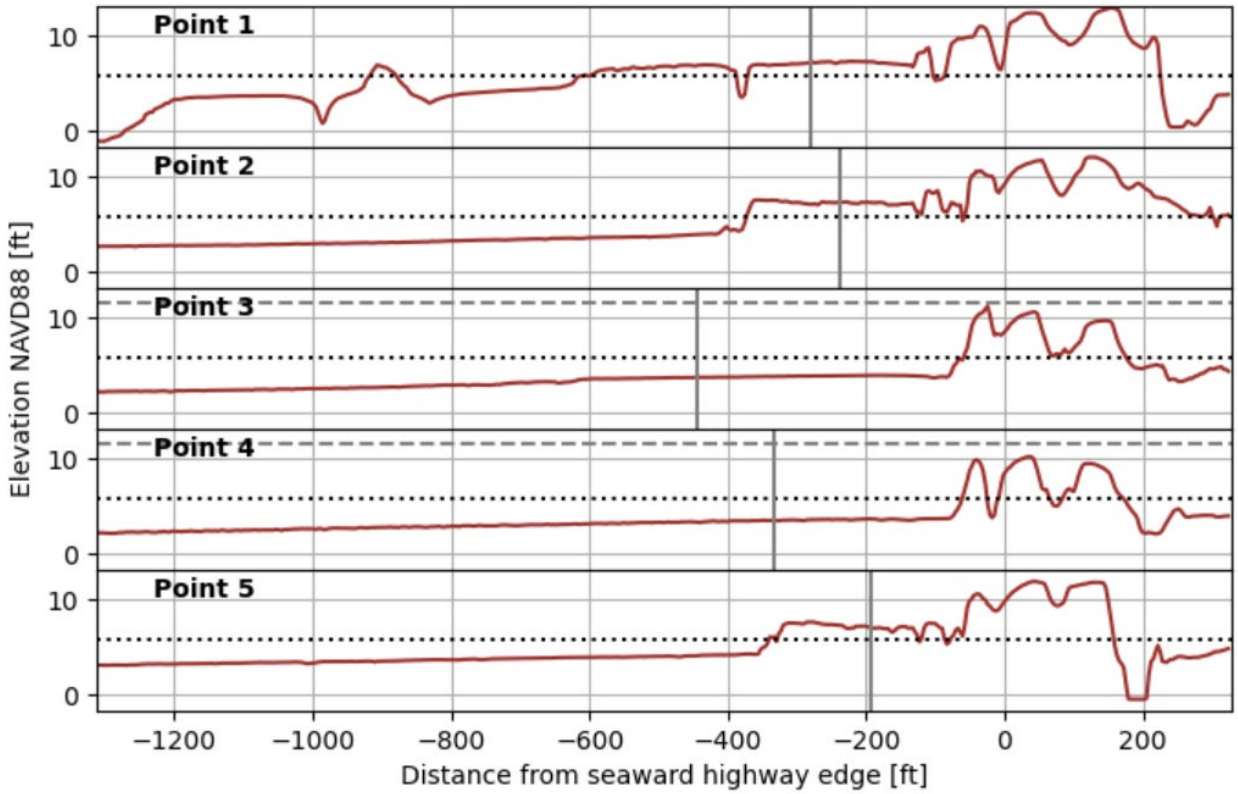

Figure 1.4.7: Elevation profiles (using the 2020 USGS CoNED TBDEM, Figure 1.3.1) along transects shown in Figure 1.4.1. The approximate delineation of mud flat and salt marsh is shown as a dotted black horizontal line. The vertical gray line shows the extraction point location. The dashed horizontal gray line shows the planned elevation of the shoreline protective structure at Points 3 and 4 when the Bay Trail Project is complete.

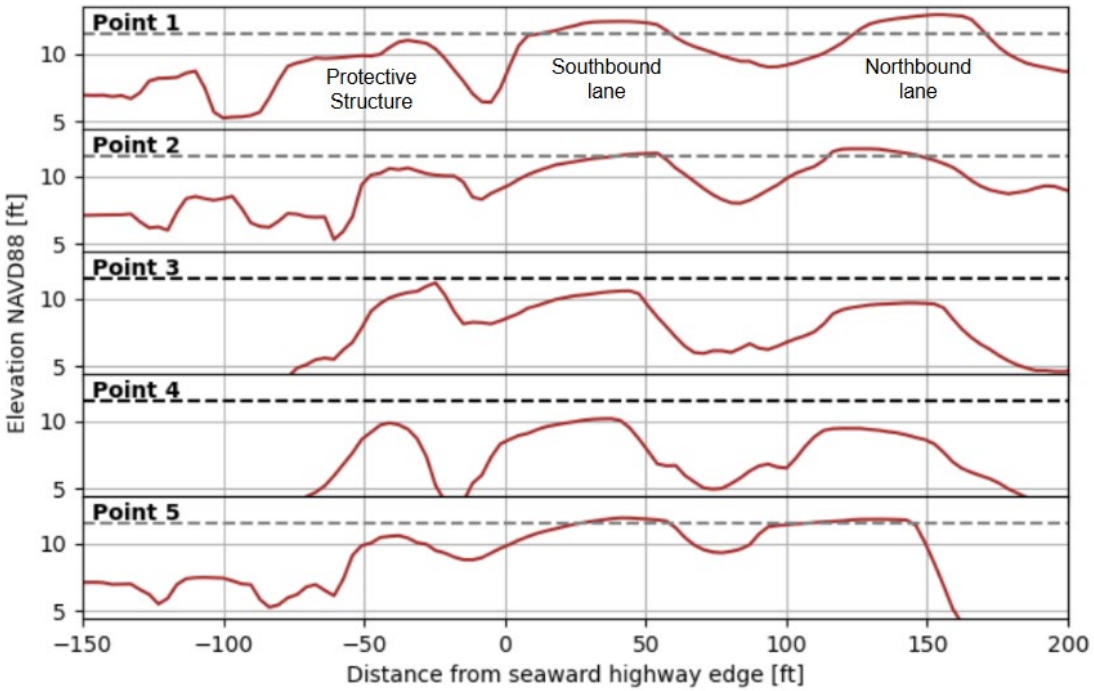

Figure 1.4.8: Elevation profiles zoomed in on the shoreline protective structure and highway lanes. The dashed horizontal lines mark 11.5 ft NAVD88, which is the planned max structure height at Points 3 and 4 once the Bay Trail is complete.

Table 1.4.2: Estimated protective shoreline structure characteristics (after Bay Trail is complete)

Point	1	2	3	4	5
Type*	ORP	ORP	RSP	RSP	ORP
Slope**	0.2	0.5	0.6	0.6	0.3
Crest Elevation [ft]**	11.0	10.6	11.5	11.5	10.6
Orientation [°]***	6	0	303	300	298
Crest Width [ft]*****	NA	NA	6.6	6.6	NA

* ORP = Old Rail Prism: grassy mud and cobble. RSP = Rocky Shore Protection: riprap

** Slope and crest elevation at points 1,2,& 5 were estimated from the 2019 CoNED TBDEM (Figure 1.3.1). Slope and crest elevation at points 3&4 were estimated from the project plans for the Bay Trail (CHDPW, 2022).

*** Orientation is the cartesian angle (0° is pointing east, 90° is pointing north, etc.) of the vector pointing normal to the structure, from the seaside of the structure toward land. Estimated using Google Earth.

**** The structure crest width is provided for RSP structures for determining overtopping discharge. It is not needed for the ORP structures (see Section 6). We estimated the RSP crest width values as larger than specified in

the project plans for the Bay Trail because the given 2ft value does not seem physically possible due to the boulder sizes.

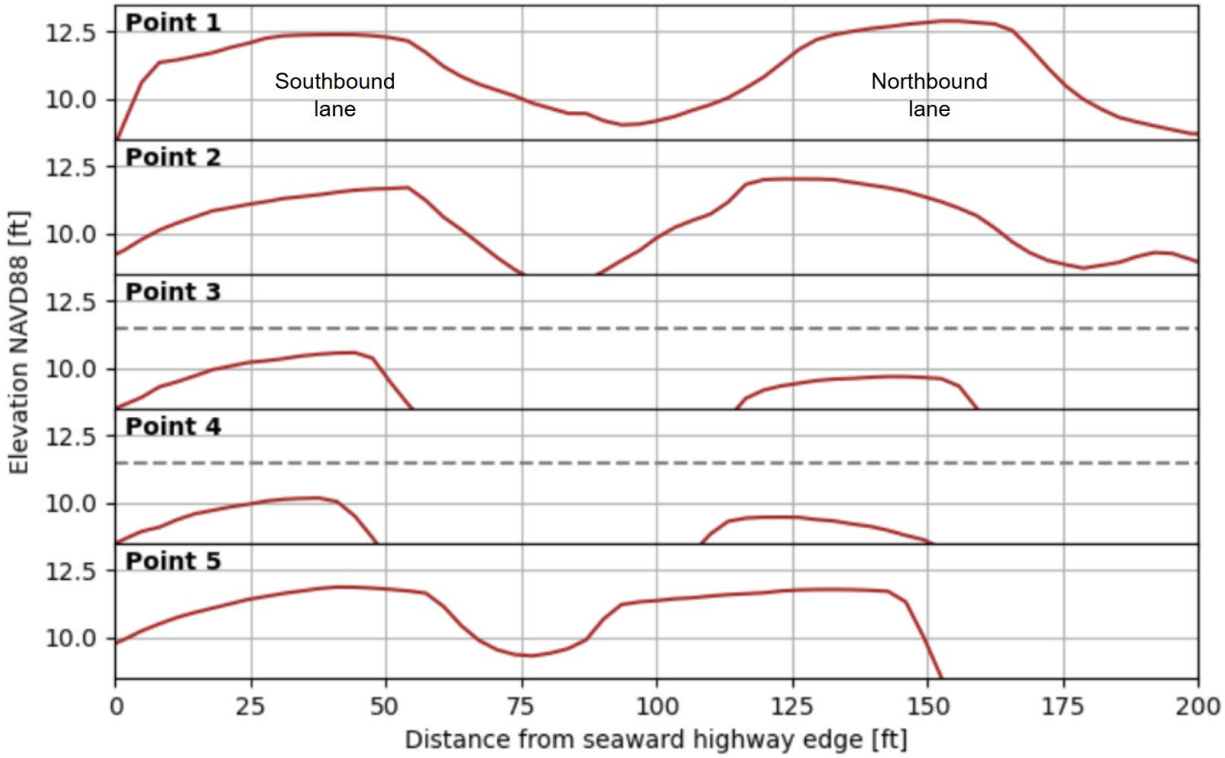

Figure 1.4.9: Profiles zoomed in on the highway lanes to emphasize the differences in elevation. The dashed horizontal lines mark 11.5 ft NAVD88, which is the planned max structure height at Points 3 and 4 once the Bay Trail is complete.

2. Sea level rise

The California Sea Level Rise Guidance (2024) describes five statewide regional SLR scenarios based on the Intergovernmental Panel on Climate Change 6th Assessment Report's framework (IPCC AR6: Masson-Delmotte et al., 2021), which uses the latest generation of global climate models from the Coupled Model Intercomparison Program's sixth phase (CMIP6). The Low scenario represents the lower edge of plausibility and aggressive emissions reductions. The Intermediate-Low scenario is the lower bound of the most likely SLR, while the Intermediate is the upper bound of the most likely SLR. The Intermediate-High scenario is associated with high emissions and low confidence ice processes, while the High scenario requires very high emissions and lots of low confidence ice processes. Low confidence ice processes include "earlier-than projected ice-shelf disintegration in Antarctica, abrupt and widespread onset of marine ice-sheet instability and/or marine ice-cliff instability in Antarctica, and faster-than-projected changes in surface-mass balance on Greenland." The previous California Sea-Level

Guidance from 2018 (Griggs et al., 2017) included an extreme "H++" scenario that is now considered outdated due to a better understanding of these low confidence ice processes. The former H++ scenario is consistently above the scientifically plausible SLR in the 2024 Update. This coastal hazards assessment considers seven sea level futures associated with these scenarios: the current condition; the 2050 Intermediate scenario; the 2100 Intermediate, Intermediate-High, and High scenarios; and the 2150 Intermediate-High and High scenarios (Figure 2.1 and Table 2.1). The 2150 Intermediate scenario is not included because the 2100 Intermediate-High and High scenarios bracket this scenario. We use the state-wide average SLR values from the 2024 California Sea Level Rise Guidance (instead of the Humboldt Bay values) because we account for vertical land motion at a more local scale (see next section).

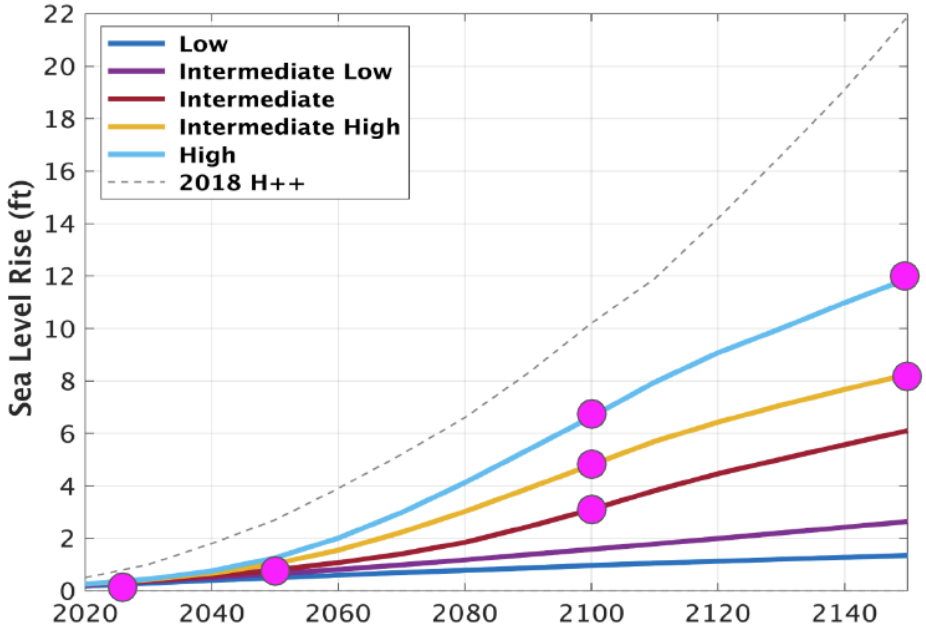

Figure 2.1: Adapted from California SLR Guidance (2024). Regional SLR scenarios for California from 2020-2150 in feet, referenced to 2000. (These projections include the statewide average VLM rate of 0.10 mm of uplift/year.) Magenta circles indicate the SLR futures considered in this report. The outdated H++ scenario (Griggs et al., 2017) is included for comparison.

Table 2.1: SLR futures considered in this report, corresponding to magenta dots in Figure 2.1.

Scenario	2023	2050	2100	2150
Current Condition	X[1]			
Intermediate		0.8 ft (0.24 m)	3.1 ft (0.94 m)	
Intermediate - High			4.9 ft (1.5 m)	8.3 ft (2.5 m)
High			6.6 ft (2.0 m)	11.9 ft (3.6 m)

2.1 Relative sea-level change and vertical land motion

The primary cause of regional differences in relative sea level rise across California is vertical land motion (VLM), especially in Wigi, due to its location at the tectonically active Mendocino Triple Junction (Figure 2.1.1). Patton et al. (2023a) used tide gauges, continuous GPS stations, and land level surveys to assess VLM in northern coastal California. They show VLM rates with the glacial isostatic adjustment (GIA) rates removed to focus on tectonic VLM, but they provide VLM rates that include GIA in the Zenodo Data Repository that was published with their paper (Patton et al. 2023b). Glacial isostatic adjustment is the land movement due to changes in glacial ice coverage. Our region's response to the last ice age's glacial retreat is uplift now that it is not weighed down by glaciers. However, GIA is only one component of VLM. Many areas in Wigi are subsiding overall due to tectonic subsidence outpacing GIA uplift. It is important to use the overall effect when calculating relative sea level rates. All figures in this report showing VLM include GIA (as well as the tectonic contributions), which is why they look slightly different from Patton et al. (2023a). Within Wigi, the largest negative VLM rates (most severe subsidence rates) are in South Bay (Figure 2.1.2). **At first glance, the land-level rates along the northern end of the Eureka/Arcata corridor appear to show uplifting, while the southern end seem to show subsidence. However, the uncertainty in these leveling point measurements span zero** (Figure 2.1.3)**. Additionally these measurements are only based on two surveys in time. Therefore, as a conservative approach, we use the Mad River Slough** (MRS) **tide gauge's VLM rate (-0.54mm) for all sites along the corridor.**

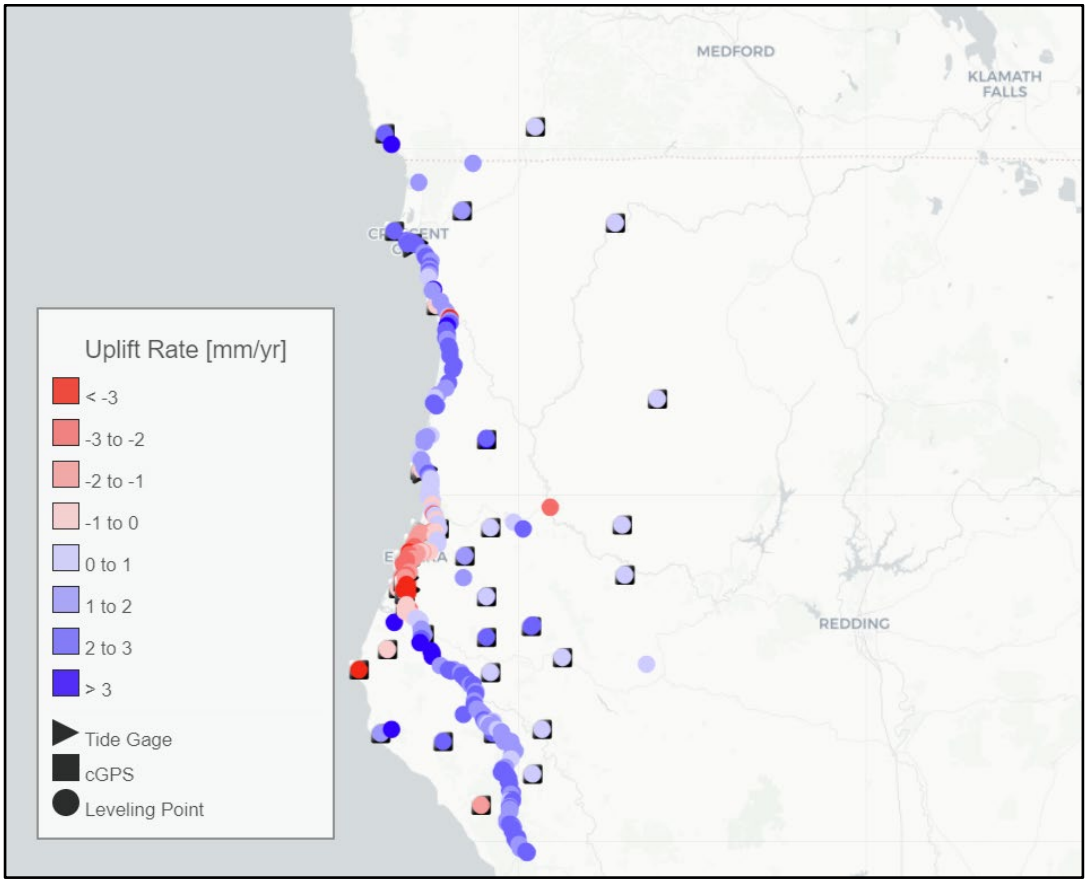

Figure 2.1.1 Regional VLM rates from Patton et al. 2023b Zenodo Repository (including GIA)

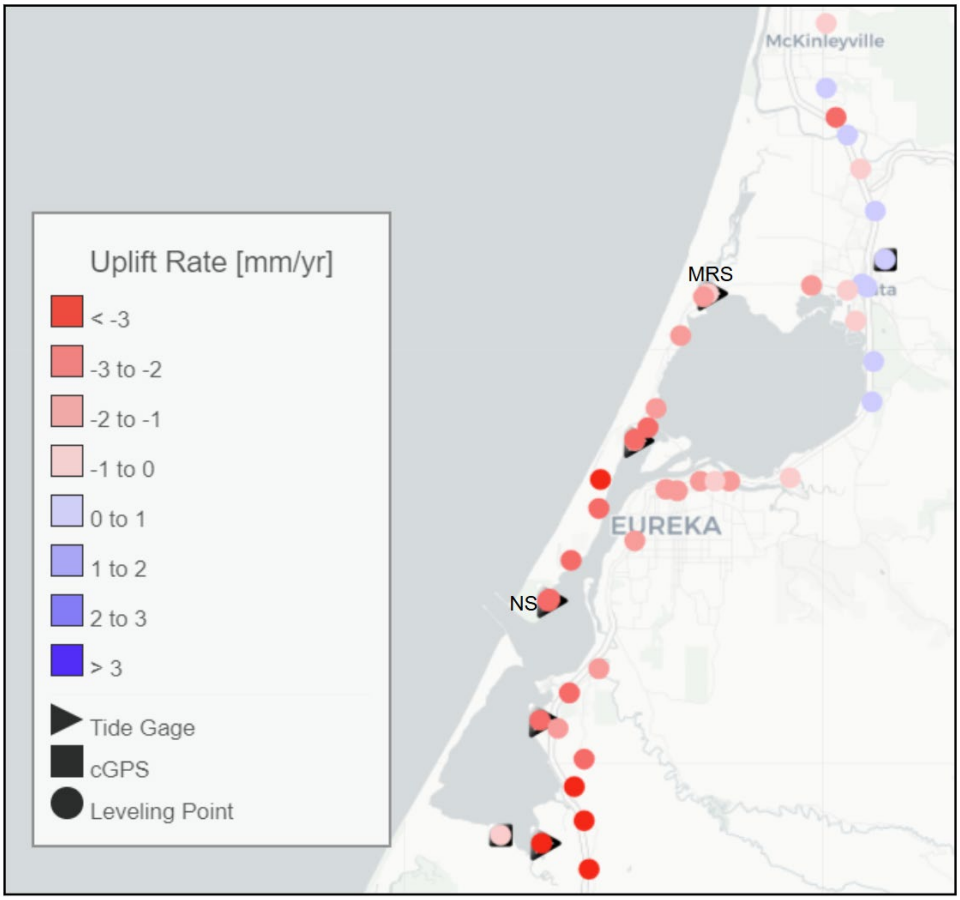

Figure 2.1.2 Wigi VLM rates from Patton et al. 2023b Zenodo Repository (including GIA)

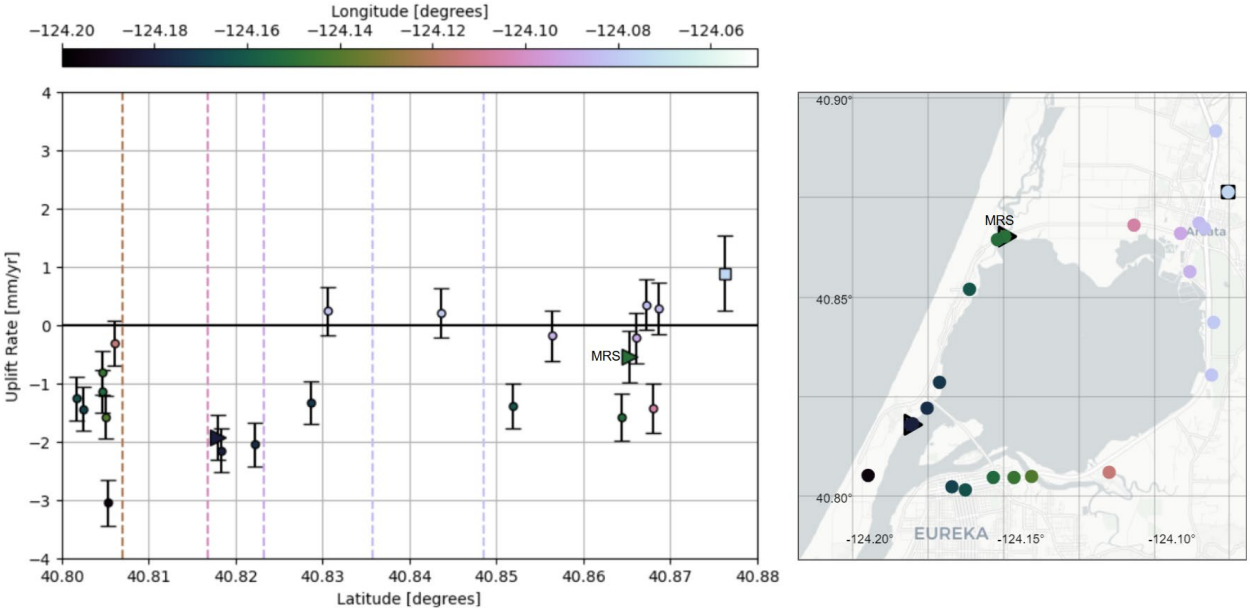

Figure 2.1.3: VLM rates and their uncertainty in Northern Wigi/Humboldt Bay (Arcata Bay) versus latitude. The colors of the dots on the plot and map correspond to the longitude location of the VLM measurement device. Latitude values of extraction points (Figure 1.4.1) are shown as dashed vertical lines on the plot, where their longitude values also correspond to the colorbar.

3. Water Level Glossary

In Figure 3.1 we provide a visual glossary of water level terminology. Mean sea level changes with relative SLR (Section 2). The astronomical tide describes water level fluctuations that result from the gravitational effects of astronomical objects, especially the sun and moon. Earth's shape and rotation also affect the timing and spatial pattern of the tides. The non-tidal residual is the variability that a tide gauge measures that is NOT the astronomical tide, nor sea level rise, nor vertical land motions. The non-tidal residual includes climate oscillations (e.g. El Niño Southern Oscillation), seasonal effects (e.g. seasonal temperature and wind patterns), and storm surge (e.g. inverse barometer effect and regional wind setup). Local wind setup, in our case, is wind setup due to wind blowing water around in the bay. Wave setup is the time-average increase in water levels due to the presence of breaking waves. (Right before waves break there is a small amount of wave setdown which is not shown in the schematic.) Swash is the uprush and downrush of water on the beach due to the presence of waves. Runup is the sum of wave setup and swash uprush combined. Typically we characterize wave runup using $R_{2\%}$, which is the elevation above a hypothetical wave-free reference water level that is exceeded by two percent of the individual wave runup events. Still water level is the water level due to mean sea level, plus the tide and the non-tide residual. Here we use the term "reference" water level as the water level due to still water level plus local wind setup. The total water level is the reference water level plus $R_{2\%}$.

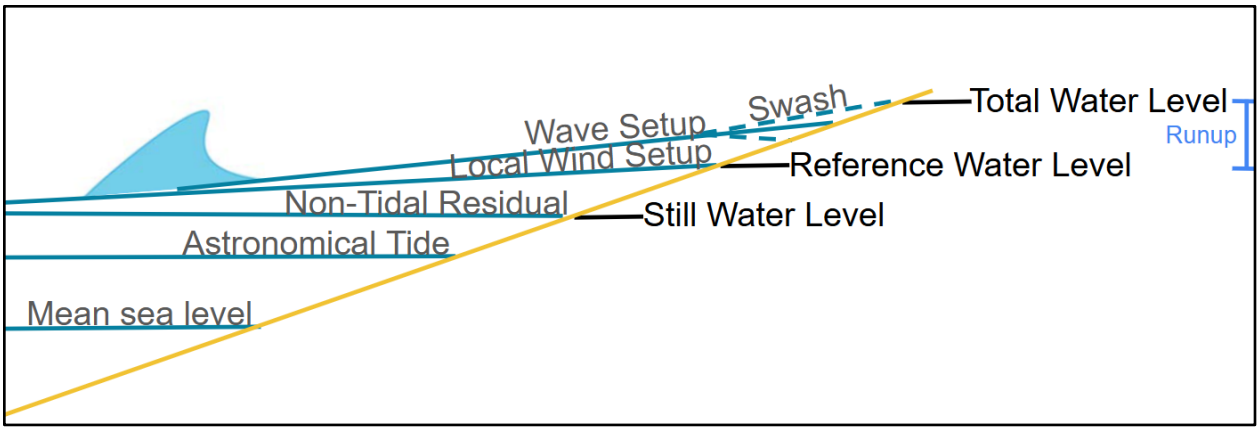

Figure 3.1: Visual glossary of water level terms.

4. Reference water levels: EFDC hydrodynamic model

As part of the Humboldt Bay sea-level rise modeling and inundation vulnerability mapping project (NHE, 2015), a two-dimensional hydrodynamic model (2D model) was developed for Humboldt Bay (Figure 4.1) to efficiently conduct long term sea-level change simulations. NHE (2015) used the 2D model to simulate a 100-year hourly time series (1913 to 2012) of still water levels in Humboldt Bay forced only by a sea-level height series open boundary condition (OBC). The 100-year still water series accounted for astronomical tides and non-tidal effects (e.g. storm surge and El Niño variability) but did not account for local wind setup in Humboldt Bay. For this assessment, the existing NHE (2015) 2D model was leveraged to simulate a 74-year hourly time series (1950 to 2023) of reference water levels (tide + storm surge + wind setup) using sea-level height and wind speed/direction series boundary conditions.

The existing 2D model was developed using the Environmental Fluids Dynamics Code (EFDC) modeling platform (Hamrick, 1992), which is a public domain model supported by the U.S. Environmental Protection Agency. The Dynamic Solutions-International, LLC (DSI) version was used, which has several enhancements (EFDC+) and a windows-based GUI (EEMS11.8) for pre- and post-processing (DSI 2023). The current version of EFDC+ allows domain decomposition of the model grid into subdomains which can be assigned separate processor cores for improved computational performance.

Results for the NHE (2015) simulations showed that the existing 2D model reproduced Humboldt Bay observed water levels at five locations (North Spit, Mad River Slough, Samoa, Fields Landing and Hookton Slough) reasonably well. Correlation coefficients between hourly water level observations and predictions for North Spit, Samoa and Fields Landing ranged from 0.993 to 0.996. Correlation coefficients for daily maximum water level observations at all five stations ranged from 0.972 to 0.987.

The curvilinear-orthogonal grid consists of 1,560 horizontal cells and one vertical layer, with an average orthogonal deviation of 2.3 degrees. Grid cells had an average size of 205.6 by 219.7 m, ranging in size from 12.7 to 678.8 m in the x-direction and 25.8 to 514.7 m in the y-direction. In general, the same model parameters from the NHE (2015) work were used in this simulation. The following parameters were assigned to the entire model domain: (1) roughness height (Z_0) of 0.005 m, (2) horizontal eddy viscosity of 0.001 m^2/s, and (3) wet/dry depth of 0.01 m. Initial condition water levels were set to the start of the sea-level height series, and initial velocities were set to zero. A 7-day model spin-up period was adequate to remove the initial condition effects.

For this analysis the model domain was split into 4 subdomains and 2 processor cores were assigned to each subdomain. The dynamic timestep option was used which allows for adaptive time steps constrained by the (1) Courant-Friedrich-Lewy (CFL) criteria, (2) positivity of advected constituents (if used), (3) rate of depth change, and (4) a maximum time step of 4 seconds. The current model configuration requires approximately 33.6 computational hours for the 74-year simulation.

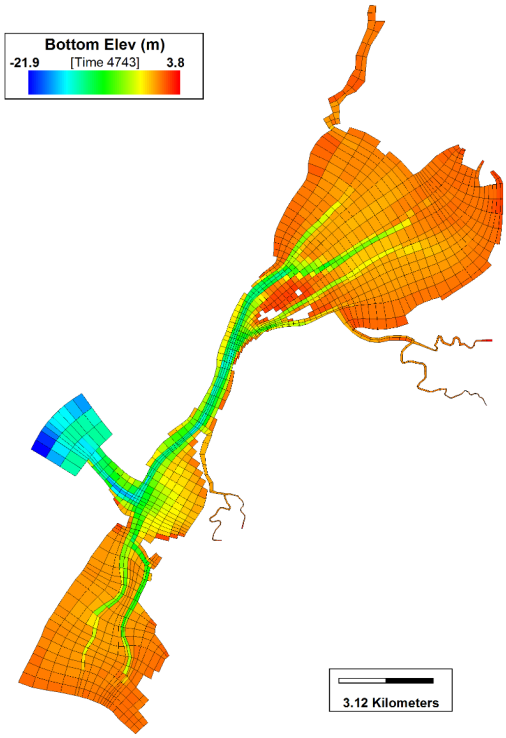

Figure 4.1: Humboldt Bay hydrodynamic model grid and bed elevations referenced to m, NAVD88 (NHE 2015).

4.1 Boundary conditions

Two boundary condition time series were developed for this assessment, consisting of a sea-level height and a wind series. Similar to the NHE (2015) work, the sea-level height series is based on the Crescent City tidal station (NOAA ID 9419750) which has a period of record from 1933 to present. The wind series was developed from observations at the Arcata/Eureka Airport spanning 1949 to present. For this assessment, the length of boundary condition time series spanned 74-years (1950 to 2023) and were constrained by the Arcata/Eureka Airport observation period of record.

Sea-level height series

A stationary 74-year hourly sea-level height series spanning 1950 to 2023 was developed using data for the Crescent City tidal station (NOAA ID 9419750). Hourly observations and astronomical tidal predictions were downloaded from NOAA COOPS (https://tidesandcurrents.noaa.gov) on station datum and then mean sea level (MSL) for the 1983-2001 tidal epoch, relative to station datum, at each site was removed, vertically referencing the time series to MSL. Flagged measurements (for inferred or out of range values) and measurements with a standard deviation greater than 0.4 meters were removed from the time series. Additionally, there were two time periods that appeared to have a clock error: April 1 1950 08:00:00 to May 1 1950 07:00:00 (GMT), and Dec 9 1978 08:00:00 to Jan 1 1979 08:00:00 (GMT). Data from these time periods was removed from our analysis and NOAA has been alerted to the issue.

The hourly observations were detrended to remove the relative sea-level rate using a least-squares linear model. Detrending effectively references the hourly data to the middle of the current 1983-2001 tidal epoch, which is midnight on 2 July 1992 (1992.5). The detrended Crescent City tide gauge time series is similar to the detrended North Spit time series (Figure 4.1.1, left) for the overlapping period of record (1977-2003). We remove the predicted astronomical tide to calculate the observed non-tidal residual (NTR) and find that these time series are also comparable between sites (Figure 4.1.1, right). Some of the major differences between sites are during tsunamis (occurring on 22 May 1960, 27 March 1964, and 11 March 2011).

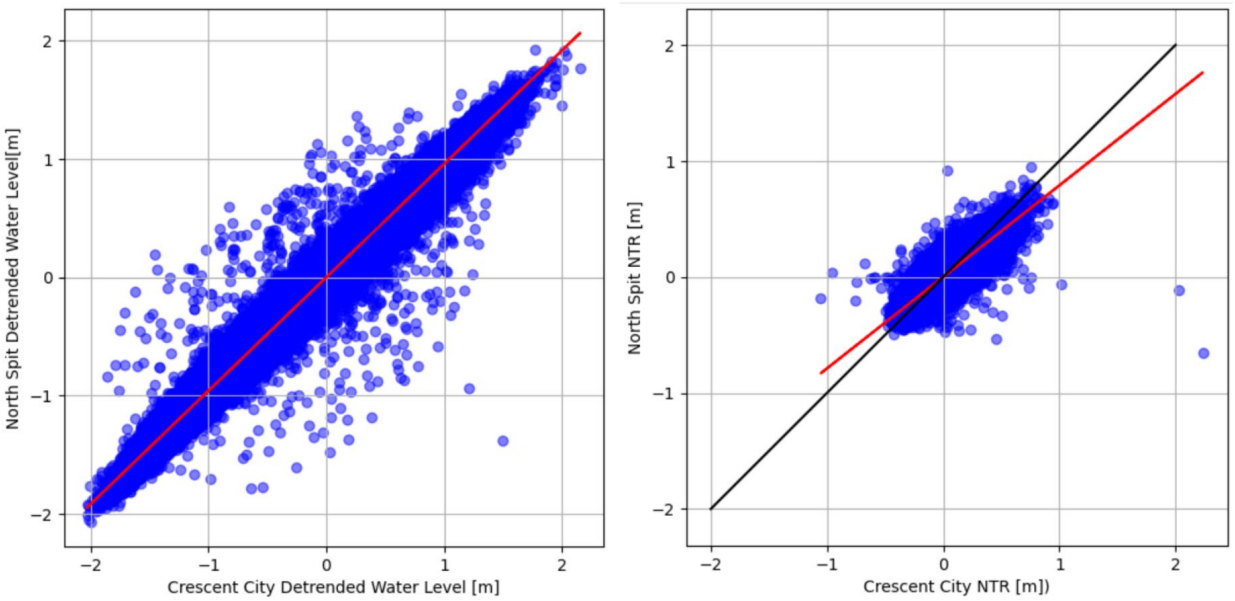

Figure 4.1.1: [Left]: Detrended North Spit water levels vs. detrended Crescent City water levels. R^2: 0.9813, Root mean square error (RMSE): 0.090m. [Right]: Observed North Spit non-tidal residual vs. observed Crescent City non-tidal residual. R^2: 0.7825, RMSE: 0.057m.

To fill in data gaps, a multiple linear regression was performed to relate the observed non-tidal residual at Crescent City to modeled winds, modeled sea level pressures, and observed ENSO state, separately analyzed by season (Winter: Dec, Jan, Feb; Spring: Mar, Apr, May; Summer: Jun, Jul, Aug; Fall: Sep, Oct, Nov). Hourly modeled wind velocity vectors (u and v) and mean sea level pressure estimates were obtained from the European Centre for Medium-Range Weather Forecasts (ECMWF) atmospheric reanalysis (version 5) at the grid location closest to Arcata Airport (ACV). This model data is referred to as ERA5 (ECMWF ReAnalysis version 5). Reanalysis models, like ERA5, blend observations and model output to better represent past atmospheric conditions. Additionally, the El Niño Southern Oscillation Oceanic Niño Index (ENSO ONI) was downloaded from NOAA NCEP (http://www.cpc.ncep.noaa.gov/data/indices/oni.ascii.txt). The ENSO ONI is a 3-month running mean of the sea surface temperature anomaly in the central tropical Pacific Ocean and this was linearly interpolated to have hourly resolution. The first eighty percent of the data was used to train the regression model and the last twenty percent was used for testing. (Results were similar when using random times for the 80%(20%) split for training(testing).) Results for all seasons are shown in Figure 4.1.2, and the testing results for individual seasons are displayed in Table 4.1.1.

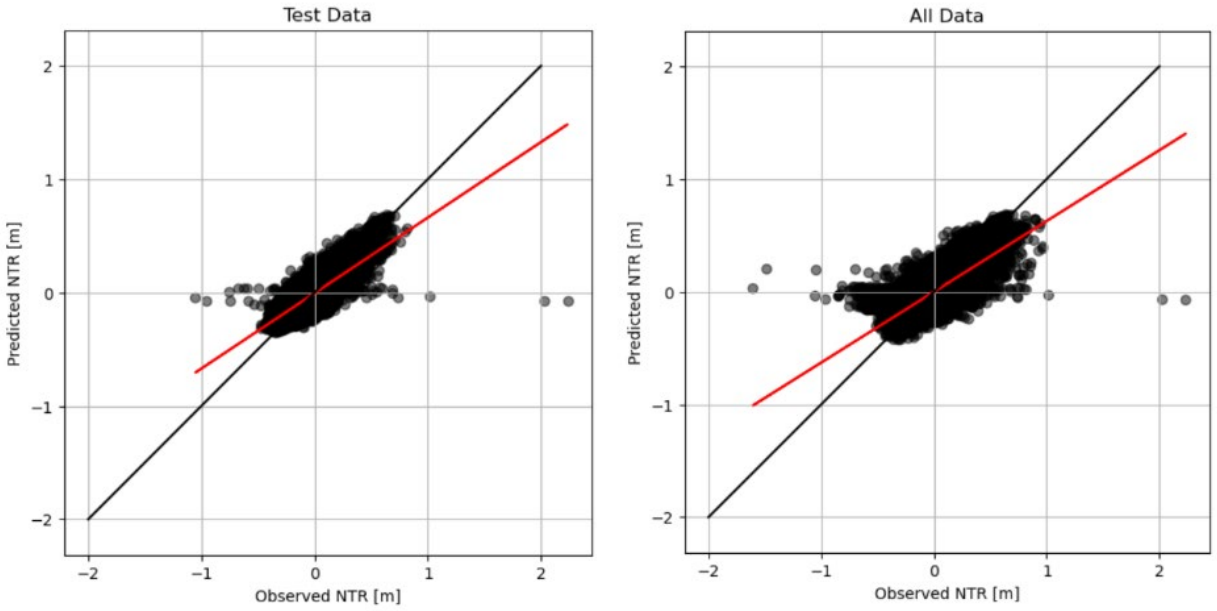

Figure 4.1.2: Predicted vs. Observed Crescent City NTR for testing data [left] and all data [right]. Testing Data R^2: 0.66; Testing Data RMSE: 0.071m; All Data R^2: 0.63; All Data RMSE: 0.076m

Table 4.1.1: Performance per season of regression model on Crescent City NTR testing data.

Season	R^2	RMSE [m]
Winter	0.75	0.084
Spring	0.58	0.079
Summer	0.36	0.052
Fall	0.60	0.063

The regression model predictions for NTR were used to fill in gaps in the observed NTR record (Figure 4.1.3, top). Then the gap filled NTR was added to the predicted tides to create a continuous 74 year water level time series relative to MSL. The resulting stationary 74-year hourly still water level series was converted from MSL to the NAVD88 vertical datum using the published NOAA and National Geodetic Survey (NGS) datum conversion (SWL_{MSL} - -1.014 m = SWL_{NAVD88}) for the Crescent City tide station (Figure 4.1.3). Recall the detrending effectively sets the mean sea level to the middle of the tidal epoch, which is 1992.

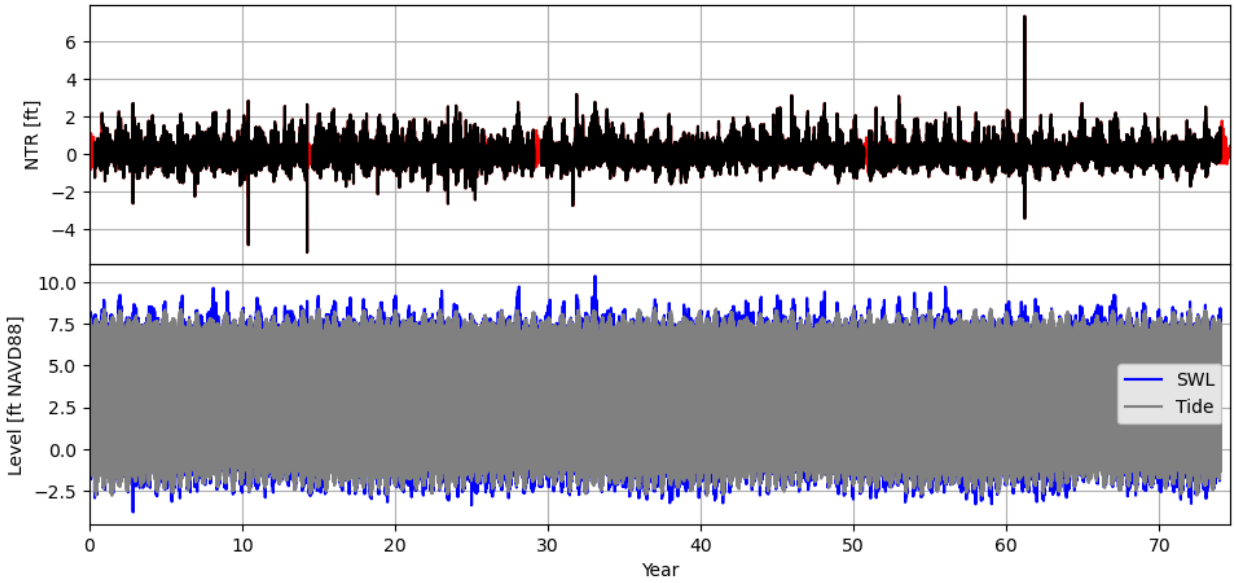

Figure 4.1.3: [Top]: Observed NTR [ft] at Crescent City (black) and gap filled (red). [Bottom]: Continuous 74-year tide (gray) and still water level (blue) time series using mean sea level from year 1992 [ft, NAVD88].

Wind speed and direction series

A 74-year hourly wind speed and direction series spanning 1950 to 2023 was developed using the Integrated Surface Data (ISD) from the Arcata/Eureka Airport (WBAN: 24283; USAF: 725945; Call: KACV) downloaded from NOAA. For this assessment the hourly (or more frequent) wind speed and direction observations were extracted from the ISD. Reported wind speeds consisted of 1-min averaged wind speed (pre-ASOS data) or 2-min average wind speed (post-ASOS data).

Processing the wind speed and direction data first consisted of removing any ISD reported suspect, erroneous, or missing data. Next adjustments must be made to account for the varying anemometer heights (Table 4.1.2).

Table 4.1.2: Record of anemometer heights at the Arcata/Eureka Airport

Date of adjustment (M/D/Y)	Height (ft)
11/28/1949	40
8/6/1950	60
1/31/1951	44

12/15/1952	48
7/30/1959	20
2/8/2001	33

The wind speed data were adjusted to 10 m (33 ft) height using the following equations (CEM 2015; Pintar et al., 2015):

$$U^* = \frac{U_z(k)}{ln(\frac{z}{z_0})} \quad \textit{Eq. 4.1.1}$$

$$U_{10} = \frac{U^*}{k} ln\left(\frac{10}{z_0}\right) \quad \textit{Eq. 4.1.2}$$

where U^* is the friction velocity, U_z is the wind speed height z above the surface, k is the von Karmen constant (~0.41), and z_0 is the roughness height at the surface (0.03 in this analysis).

The 1-min or 2-min wind data were then adjusted to 1-hour duration using the following equations (CEM 2015):

$$\frac{U_t}{U_{3600}} = 1.277 + 0.296 \tanh(0.9 \log(45/t)) \quad \text{for } t < 3600s \quad \textit{Eq. 4.1.3}$$

$$\frac{U_t}{U_{3600}} = 1.5334 - \log(t) \quad \text{for } 3,600 < t < 36,000s \quad \textit{Eq. 4.1.4}$$

with wind speed t, U_t the wind speed at specified duration, and U_{3600} the 1-hour (3,600 s) wind speed. Further adjustments to fetch-limited conditions were not made because GHD et al. (2022) showed this occurring at times on the order of an ~hour (80-87 mins, and did not vary significantly with water level) so the 1-hour duration winds were considered approximately fetch-limited conditions.

Additionally, the wind speeds were multiplied by a factor of 1.2 to account for the difference of wind speed over water compared to land (for fetch lengths <16km, CEM, 2015).

Missing hourly wind speed and direction observations were filled using ERA5 data. Figure 4.1.4 shows the hourly wind speed, and Figure 4.1.5 shows the wind rose for the 74-year wind speed and direction time series.

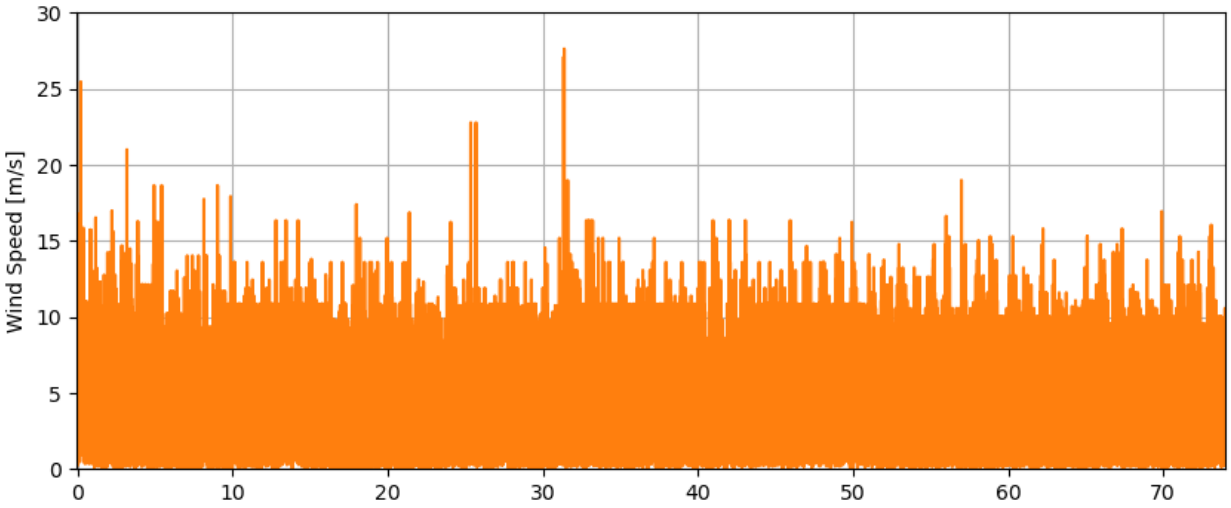

Figure 4.1.4: Wind speed (mps) for the 74-year (1950-2023) series (Arcata/Eureka Airport).

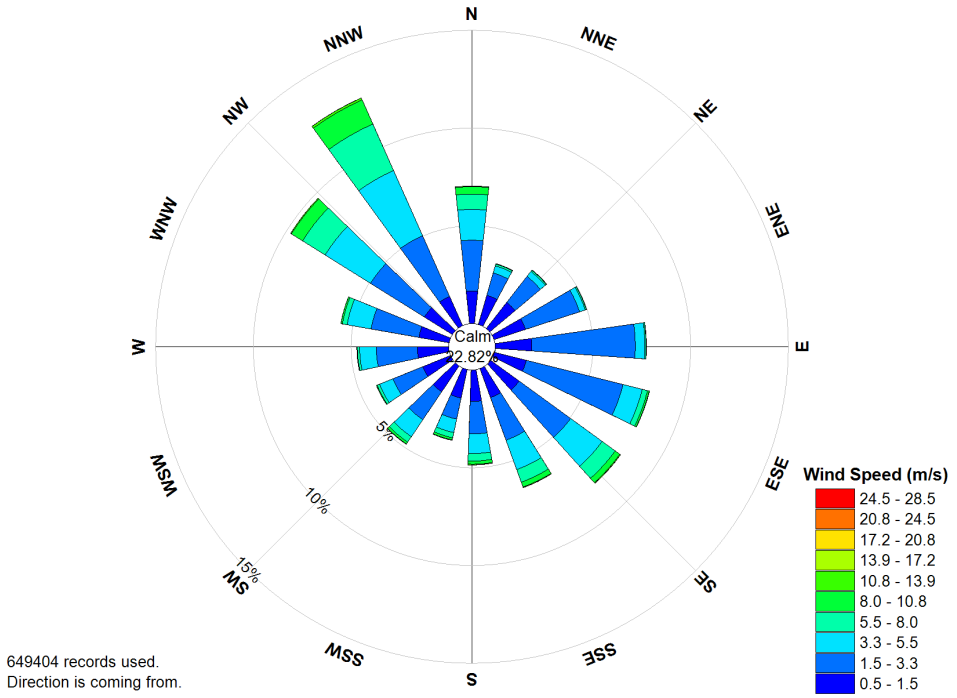

Figure 4.1.5: Wind rose for the 74-year (1950-2023) wind speed series (Arcata/Eureka Airport).

4.2 Water level response

Results from the 2D model simulations demonstrate how tidal hydrodynamics and general circulation patterns affect water levels in Humboldt Bay. Costa and Glatzel (2002) noted that tidal amplification and phase lag occur within the bay based on distance from the entrance. Simulated maximum daily water levels for a condition with no or low wind speeds shows tidal amplification of water levels in the bay (Figure 4.2.1), which has a phase (not shown) that lags with distance from the harbor entrance. **Modeled maximum tidal amplification occurs in North Bay and along portions of the corridor, where the peak still water levels are about a half a foot larger than the entrance boundary condition.**

Wind stress on the water surface from higher speed winds can generate relatively large wind setup conditions that can locally affect water levels in Humboldt Bay. Figure 4.2.2 shows the modeled wind setup (difference between water levels with and without wind) for a 20 meter per second (44.7 mile per hour) wind from the northwest and south-southwest directions. Winds from the northwest create a strong water surface gradient across North Bay as water is pulled from the west shoreline and pushed towards the easterly corridor shoreline. Winds from the south-southwest direction push water out of South Bay into North Bay, and somewhat surprisingly can create larger wind setup values along the corridor shoreline than winds blowing perpendicular to the shoreline (from the northwest). **In addition to the tidal amplification, model results show that wind setup can elevate water levels along the corridor by another couple feet, where differences in reference water levels between extraction points are typically on the order of centimeters** (Figure 4.2.3).

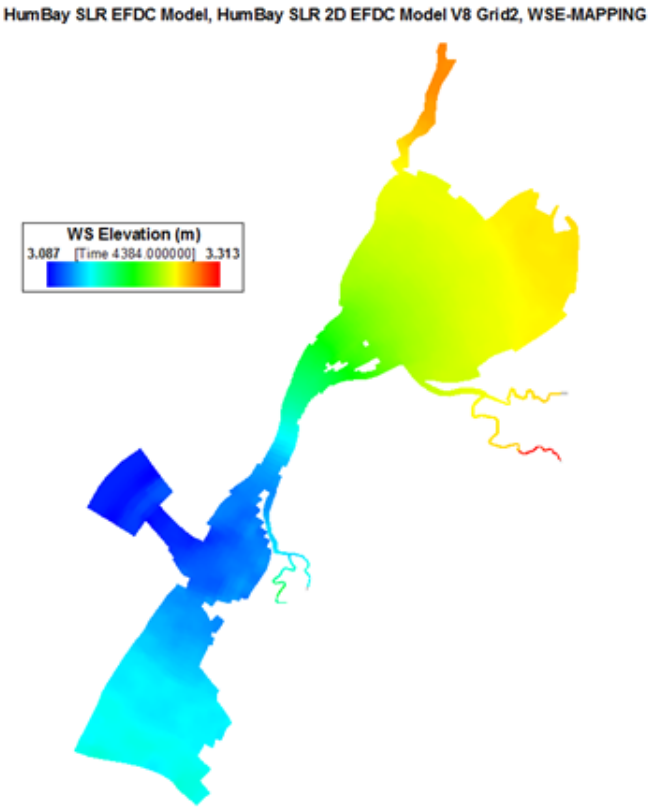

Figure 4.2.1: Simulated maximum daily still water levels (low wind conditions).

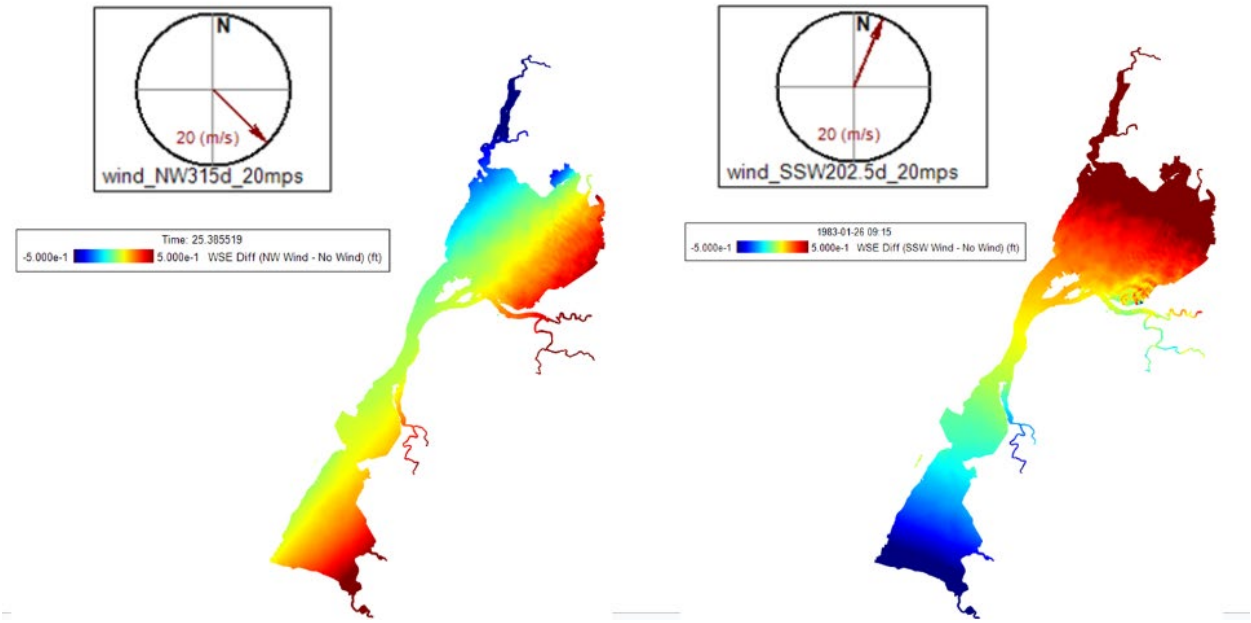

Figure 4.2.2: Example model output for a 44.7 mph (20 mps) NW wind [left] and a 44.7 mph SSW wind [right].

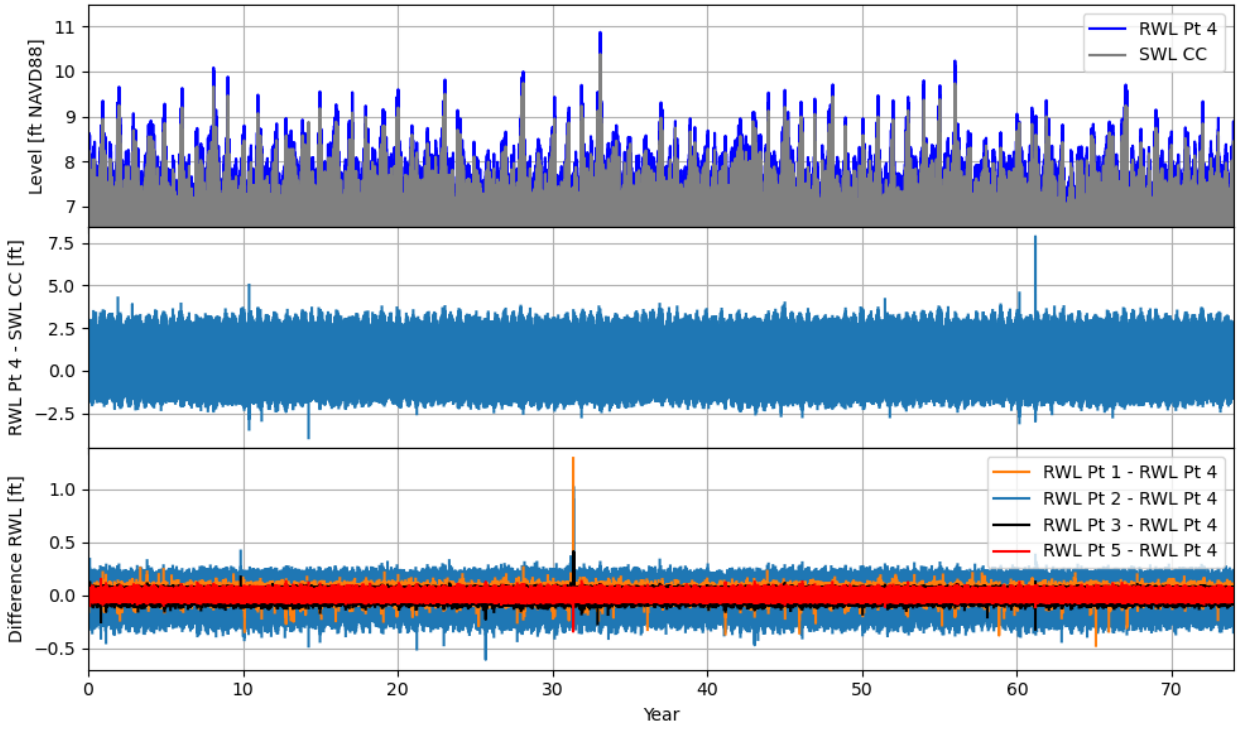

Figure 4.2.3: [Top] Reference water level time series at Point 4 compared to boundary condition still water level from Crescent City, zoomed in on high water levels. Both time series use MSL from 1992 Crescent City tide gauge [ft, NAVD88]. [Middle]: Difference between time series in the top plot [ft]. [Bottom] Difference between reference water level at each extraction point compared to Point 4 [ft].

4.3 Relative SLR adjustments

At each extraction point (Figure 1.4.1) a 74-year time series of reference water levels (Figure 3.1) was obtained from the EFDC 2D model simulations. For these time series, there is no trend in the mean sea level because the trend was removed from the boundary condition (Figure 4.1.3, bottom). This is intentional because we want to reconsider the record of historical storms occurring at a *particular* sea level. In order to explore the influence of storms at future sea levels, the reference water levels were adjusted for each sea level future (incorporating both SRL and VLM, Section 2).

The future SLR values ($FSLR_{2000\ with\ CA\ VLM}$, Figure 2.1, Table 2.1) include the statewide average of vertical land motion,VLM_{CA}, which is 0.1mm/year of uplift:

$$FSLR_{2000\ with\ CA\ VLM} = FSLR_{2000} - (future\ year - 2000)VLM_{CA} \qquad \textit{Equation 4.3.1}$$

We can recover the future SLR values without VLM using Equation 4.3.2:

$$FSLR_{2000} = FSLR_{2000\ with\ CA\ VLM} + (future\ year - 2000)VLM_{CA} \qquad \textit{Equation 4.3.2}$$

The EFDC generated reference water level time series for the highway locations ($RWL_{1992\ Hwy}$) are effectively referenced to the middle of the current 1983-2001 tidal epoch due to the detrending, which is midnight on 2 July 1992. Therefore, the future SLR values ($FSLR_{2000}$, Figure 2.1, Table 2.1) which were originally relative to 2000, were adjusted to 1992 by adding 0.0139m following Section 2.4 of Sweet et al. (2022) (Equation 4.3.3). We used higher precision than in Sweet et al. (2022)'s Table A1-2 by downloading the regional tide gauge data at: https://sealevel.globalchange.gov/national-sea-level-explorer/?type=regional&region=SWC&scope=section_1. For this we calculated a quadratic fit, and extracted the value for 1992, since these data are relative to 2000.

$$FSLR_{1992} = FSLR_{2000} + 0.0139m \qquad \textit{Equation 4.3.3}$$

Finally we calculate future RWLs along the corridor (Equation 4.3.4) using this $FSLR_{1992}$ value and the Mad River Slough VLM estimate, VLM_{MRS} = -0.54mm/year (Section 2.1).

$$RWL_{future\ year\ Hwy} = RWL_{1992\ Hwy} + FSLR_{1992} - (future\ year - 1992)VLM_{MRS} \qquad \textit{Equation 4.3.4}$$

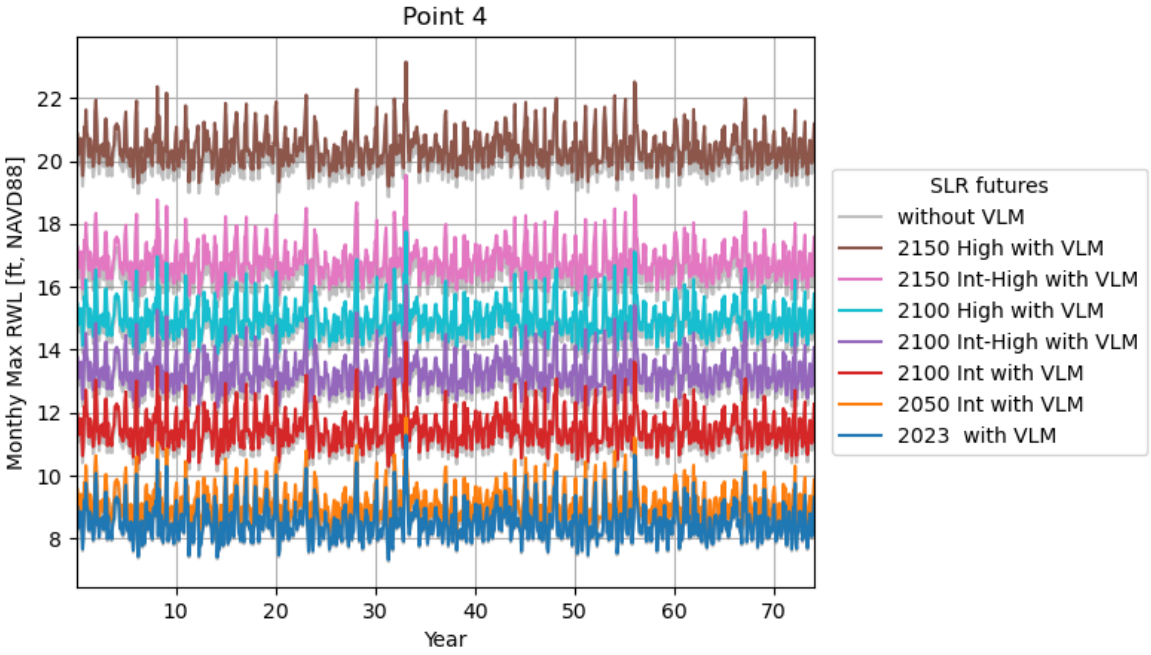

Figure 4.3.1: Monthly maximum reference water level series at Point 4 adjusted to different SLR futures, including VLM (colors) and without VLM (gray).

4.4 Reference water level return intervals

An extreme value analysis (EVA) was conducted on the daily maximum reference water-levels (RWLs) at the 5 locations using the peaks-over-threshold (POT) approach and Generalized Pareto Distribution (GPD) for each sea level rise scenario. A theoretical definition, more detailed information, and an explanation of the parameter estimation process for the POT and GPD can be found in Coles (2001). The EVA and parameter estimation were conducted with the python package pyextremes (version 2.3.3) developed by George Bocharov. All model distribution parameters were determined with the maximum likelihood estimation approach (Coles 2001). For this analysis, the threshold value was set to 97% of the maximum daily data. To satisfy the independence requirement of the EVA analysis, a de-clustering time of 3 days was used. Using these threshold and de-clustering values results in a mean number of exceedances per year that range between 3.8 to 5.5, which is consistent with recommendations for regional and global extreme sea level analysis (Arns et al., 2017). **Results show that by the 2100 Intermediate future, modeled RWLs are regularly above the crest height elevations at all locations, suggesting the existing highway will be regularly flooded at this SLR future.** (Figures 4.4.1-5)**.**

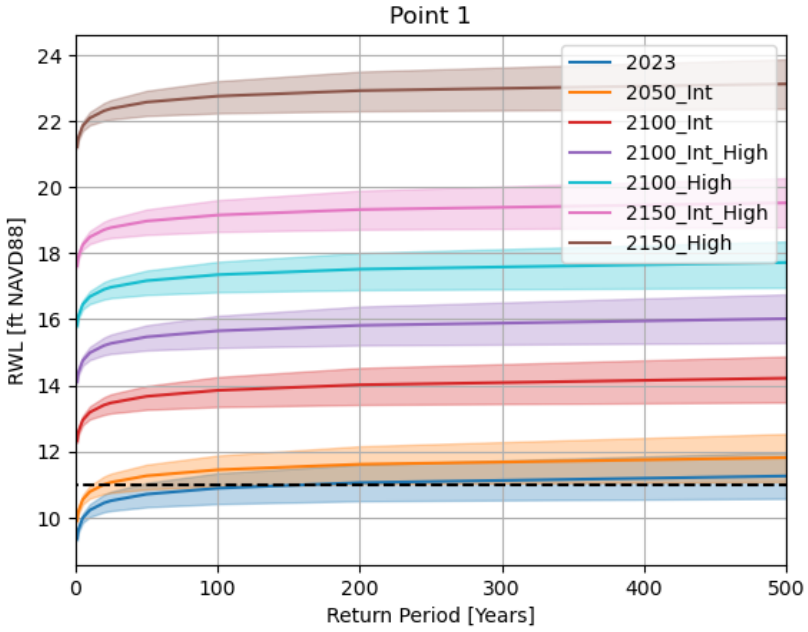

Figure 4.4.1: Estimated RWL return values vs. return period at Point 1 for various sea level futures (see legend). Shading represents the 95% confidence interval. The crest height of the structure at this location is shown as a black dashed horizontal line.

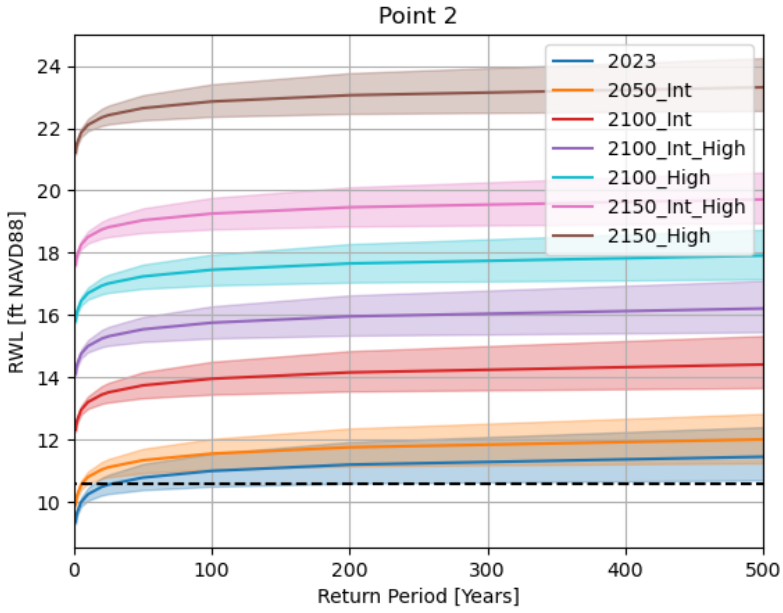

Figure 4.4.2: Same as Figure 4.4.1 but for Point 2.

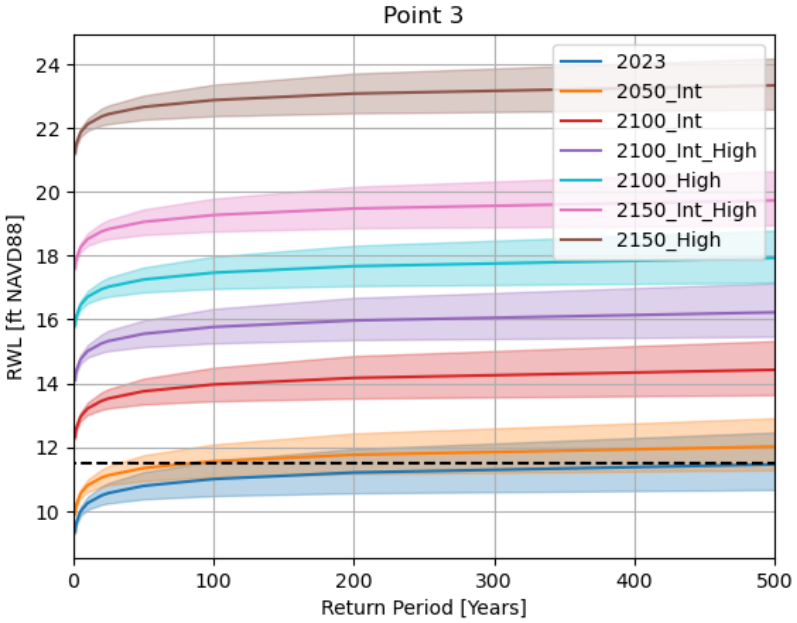

Figure 4.4.3: Same as Figure 4.4.1 but for Point 3.

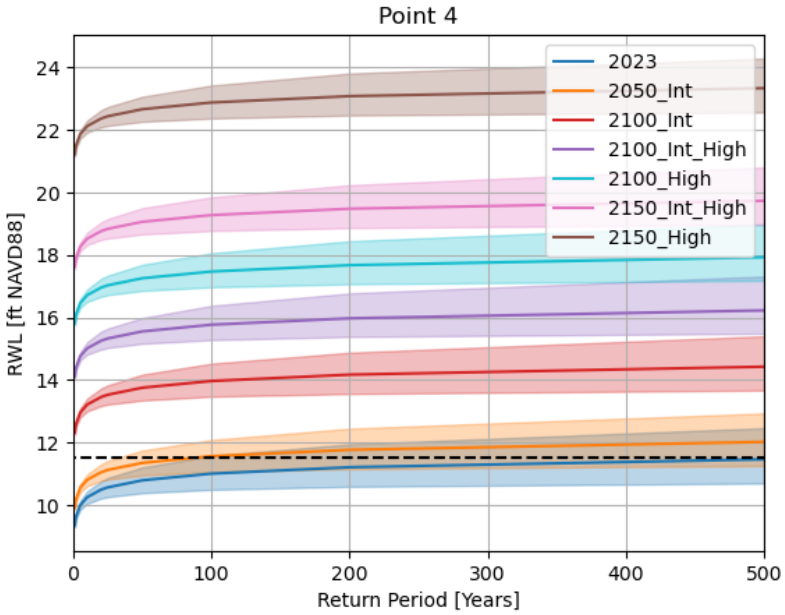

Figure 4.4.4: Same as Figure 4.4.1 but for Point 4.

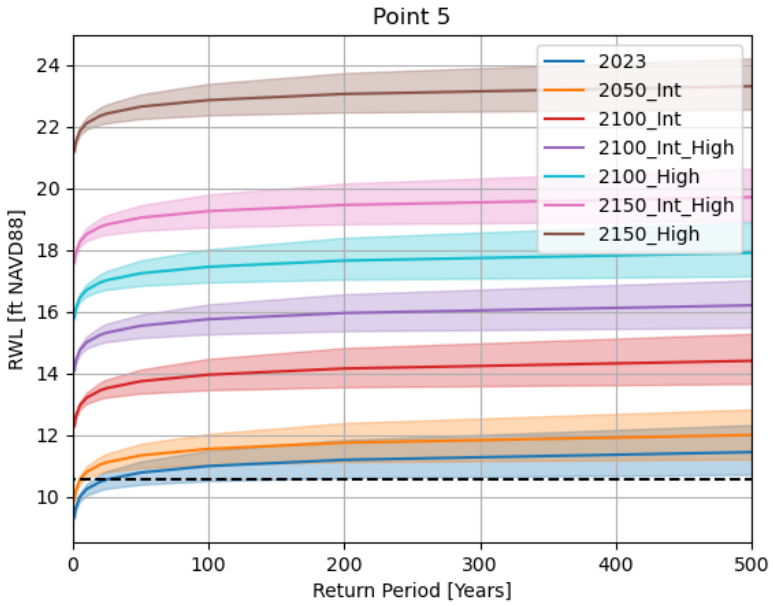

Figure 4.4.5: Same as Figure 4.4.1 but for Point 5.

5. Local wind waves: SWAN wave model

This study uses the third generation numerical wave model Simulating WAves Nearshore (SWAN; Booij et al., 1999) version 41.45AB (SWAN Team, 2024) in 2D stationary mode to simulate random short-crested wave generation by local winds, and their propagation and dissipation across the bay. Waves are described using the two-dimensional wave action density spectrum (Hasselmann et al., 1973). The directional space is discretized into 24 directional bins, and the frequency space into 29 frequency bins with a logarithmic resolution over the range 0.035 to 0.505 Hz.

Since wave data is not available at this site, calibration and validation of the model is not possible, so mostly the default configuration and parameters are used. The utilized defaults are described in this paragraph. The initial wave spectra are determined from the local wind velocities and a fetch matching the model domain's average grid size. The initial spectral shape is a JONSWAP $\cos^2$-directional distribution, and the deep-water growth curve of Kahma and Calkoen's (1992) is used with cut off values for significant wave height and peak frequency following Pierson and Moskowitz (1964). Triad wave-wave interactions are modeled by the Distributed Collinear Triad Approximation methods of Booij et al. (2009), and quadruplet interactions following the Discrete Interaction Approximation of Hasselmann et al. (1985). The dissipation of wave energy by white-capping follows Komen et al. (1984). The Battjes and Janssen (1978) formulation for dissipation due to depth-induced wave breaking is used with $\gamma = 0.73$ (breaker index), and $\alpha = 1$ (proportionality coefficient of the rate of dissipation). SWAN performs iterations as it converges on a solution and the NUM STOPC command was used to determine

when to stop the iterations (ideally when the model converges on the solution). As the solution approaches convergence, the second derivative of the significant wave height (Hs) of the iteration curve tends toward zero. SWAN stops the process if the relative change in Hs from one iteration to the next is less than "drel" (where we use the default drel=0.01) *and* the second derivative of the Hs iteration curve normalized with Hs is less than "curvat" (where we use the default curvat=0.005) *or* the absolute change in Hs from one iteration to the next is less than "dabs" (where we use the default dabs=0.005m). Both conditions need to be fulfilled in more than "npnts"% of all wet grid points (where we use the default of npnts =99.5%).

A few non-default settings were used, as described in this paragraph. The JONSWAP bottom friction formulation of Hasselmann et al. (1973) is used with a friction coefficient of 0.019 m^2/s^3 to represent the smoother mudflat bed, as suggested by the manual (SWAN Team, 2024). (We also tested a Colins friction factor of 0.015 (Colins, 1972) for a subset of runs spanning our range of use, as suggested by Mariotti & Fagherazzi (2013) for the Willapa Bay mudflats. Results appeared similar and this was not further explored.) Vegetation dissipation was implemented across the salt marsh regions using Dalrymple's formula (1984) as implemented by Suzuki et al. (2012). The plant height, plant diameter, number of plants per square meter, and the drag coefficient are 1.2192 m, 0.0067 m, 365 stems/m^2, and 0.5 respectively using measurements near the Elk River (Caltrout et al., 2019). A slightly dispersive numerical scheme is used with first order upwind, backward in space, backward in time calculations (BSBT; Whitham, 1974; and Holthuijsen, 2007) to be conservative about ensuring numerical stability considering the curvilinear grid. We also set the max number of iterations in the NUM STOPC command (described above) to 100 to be conservative (whereas the default is 50).

A curvilinear grid was used to better represent the curvature of the bay shoreline, where care was used to keep grid cell aspect ratios near 1:1 (Figure 5.1). Some cells had higher aspect ratios so we performed a test to ensure that this did not cause a numerical issue. Comparing curvilinear grid output to cartesian grid output using 25mx25m grid resolution for a 20mps wind from the northwest (315°) showed similar results. The model domain only encompasses Wigi and does not extend into the ocean because we assume that ocean waves entering through the harbor are dissipated before they reach the project area in Arcata Bay (Northern Wigi).

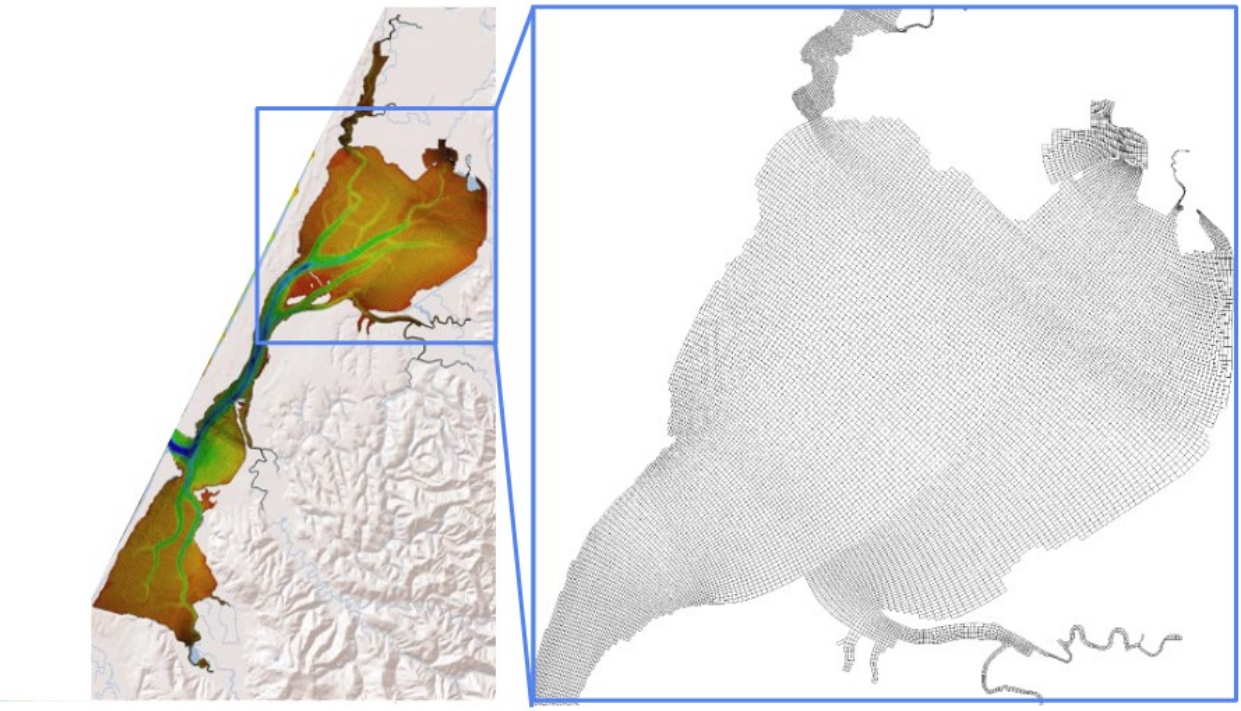

Figure 5.1: SWAN model grid for Wigi, where the zoomed in region shows Arcata Bay (North Wigi).

5.1 Look-up table

For computational efficiency we use a look-up table (LUT) approach to develop wave time series (Crosby et al. 2023). The possible forcing conditions (wind speed, wind direction and water level) are discretized, then each set of conditions is run (only once) to generate the LUT, and the full wave time series is created by querying the LUT for the given forcing conditions. The LUT discretization for each forcing condition is: wind direction from 0 to 360°, in 22.5° increments; wind speed from 3 to 33 m/s in 3 m/s increments; and water levels from 1.5 to 3m in 0.5m increments, and 3.2 to 5.6m in 0.2m increments. Figures 5.1.1 and 5.1.2 show examples of SWAN model output highlighting wave dissipation over the salt marsh, where depth limited wave breaking dominates.

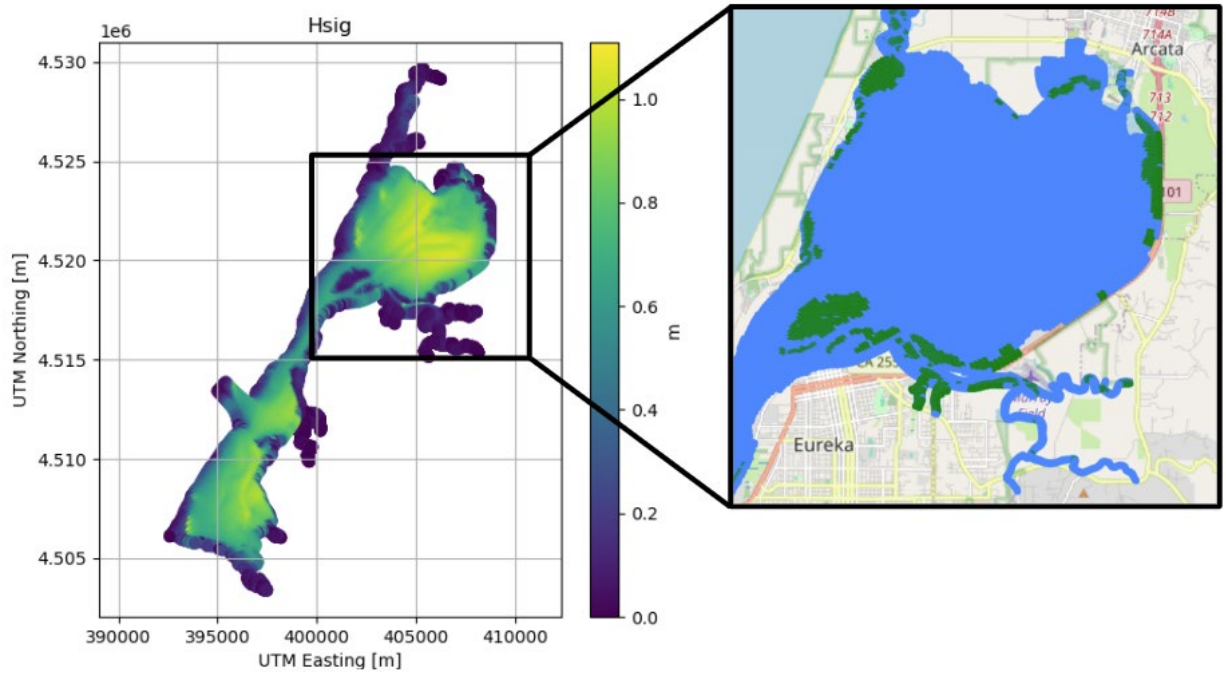

Figure 5.1.1: [Left]: Example of significant wave height from SWAN model run for the LUT node representing a 9.8 ft water level NAVD88 with a 45 mph (21 mps) westerly wind (blowing toward the east). [Right]: Modeled salt marsh locations mapped in green. Note the reduction in wave height due to depth limited wave breaking over the salt marsh.

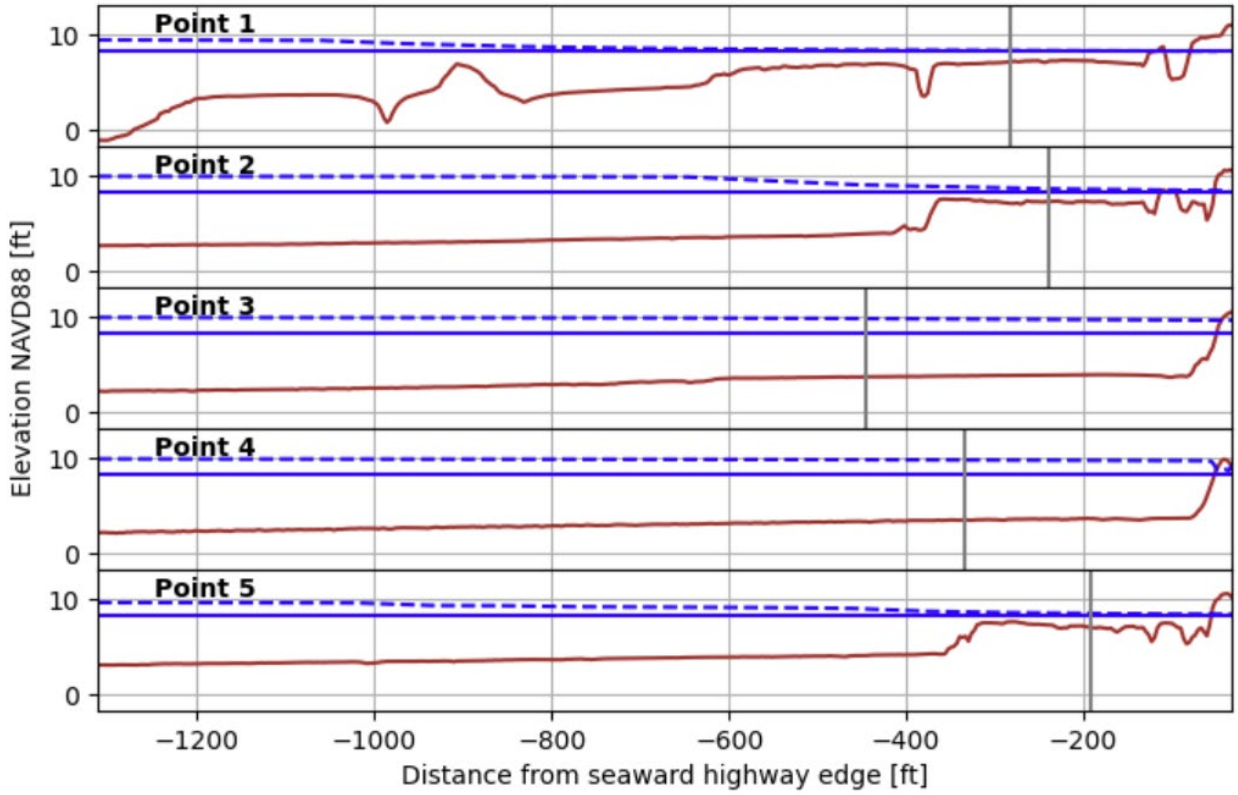

Figure 5.1.2: Significant wave height profiles (dashed blue lines) at the extraction points (Figure 1.4.1) for a 26.8 mph (12 mps) westerly wind (blowing toward the east) with a water level of 8.2 feet (solid blue lines). The locations of the extraction points are marked with a vertical gray line. Note the reduction in wave height due to depth limited wave breaking over the salt marsh at Points 1, 2, and 5.

We generate LUTs for the 5 extraction points (Figure 1.4.1) along the corridor. Example LUTs for location 4 of significant wave height, peak wave period, and wave direction are shown in Figures 5.1.3-5. Typically the largest and longest period waves occur for strong winds perpendicular to shore.

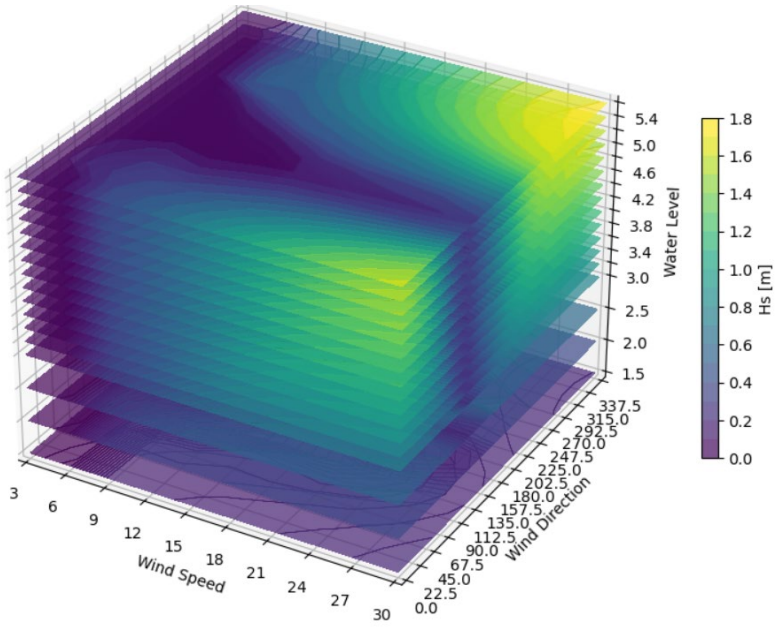

Figure 5.1.3: Example of LUT for significant wave height at Point 4 (Figure 1.4.1). Wind direction is in cartesian coordinates such that a westerly wind (blowing towards the east) = 0 degrees.

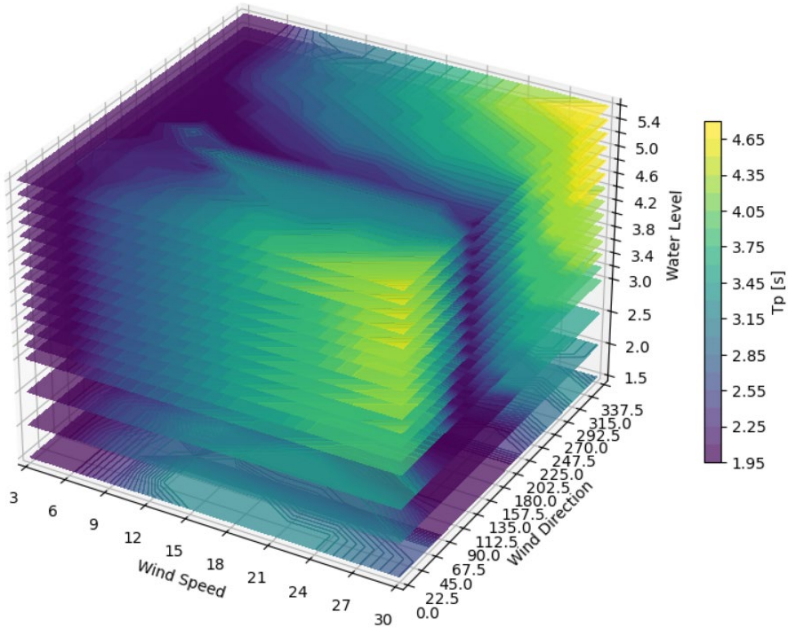

Figure 5.1.4: Example of LUT for peak wave period at Point 4 (Figure 1.4.1). Wind direction is in cartesian coordinates such that a westerly wind (blowing towards the east) = 0 degrees.

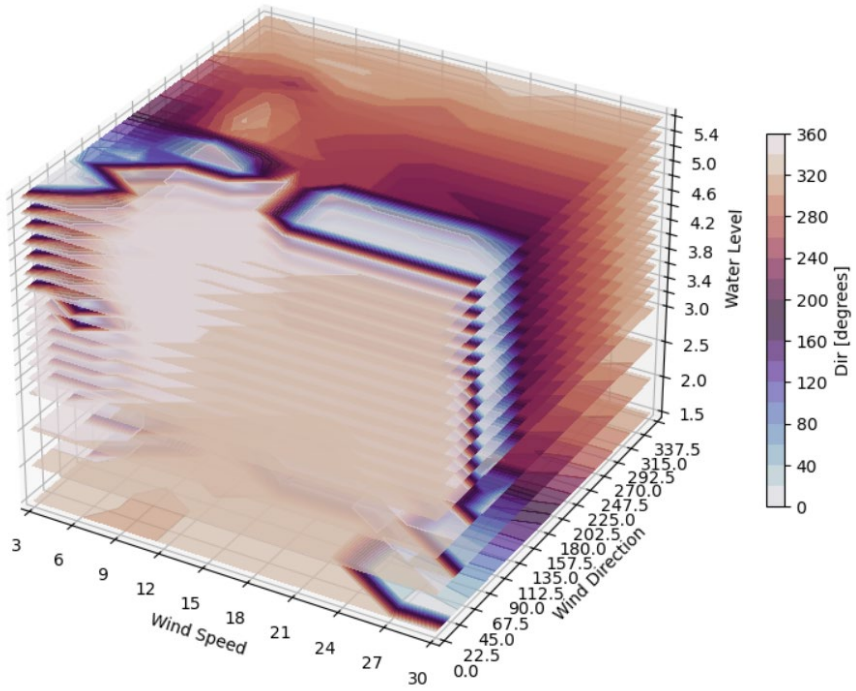

Figure 5.1.5: Example of LUT for peak wave direction at Point 4 (Figure 1.4.1). Wind and wave directions are in cartesian coordinates such that a westerly wind (blowing towards the east) = 0 degrees.

5.2 Time series of bulk wave parameters

Time series of bulk wave parameters (wave height, period and direction) at each extraction point were generated by querying the LUT based on the forcing conditions: wind speed, wind direction and water level. The same time series that was used to force the EFDC model was used for the wind queries, and the reference water levels for each extraction point and each sea level future were used for water level queries. The forcing conditions from each time step typically do not fall exactly on a LUT node, so the wave parameter at that time step was extracted from the LUT using 3D linear interpolation. **In Figures 5.2.1-2 we only show the first few SLR futures because by the 2100 Intermediate future the highway will flood regularly even without waves. The largest waves in the project area are about 2 feet tall by the 2050 Intermediate SLR future** (Figure 5.2.1, top) **and have wave periods of a few seconds** (Figure 5.2.1, middle)**. Waves tend to be larger with higher water levels due to less depth-limited breaking** (Figure 5.2.1, top)**. Higher water levels can also expose the shoreline to waves coming from additional directions** (Figure 5.2.1, bottom)**. Also note that waves are largest at Points 3 and 4 where there is no salt marsh fronting the shoreline** (Figure 5.2.2)**. The shallow salt marsh induces more depth limited wave breaking,**

such that Points 1, 2, and 5 rarely experience waves larger than half a foot by the 2050 Intermediate SLR future (Figures 5.2.1-2).

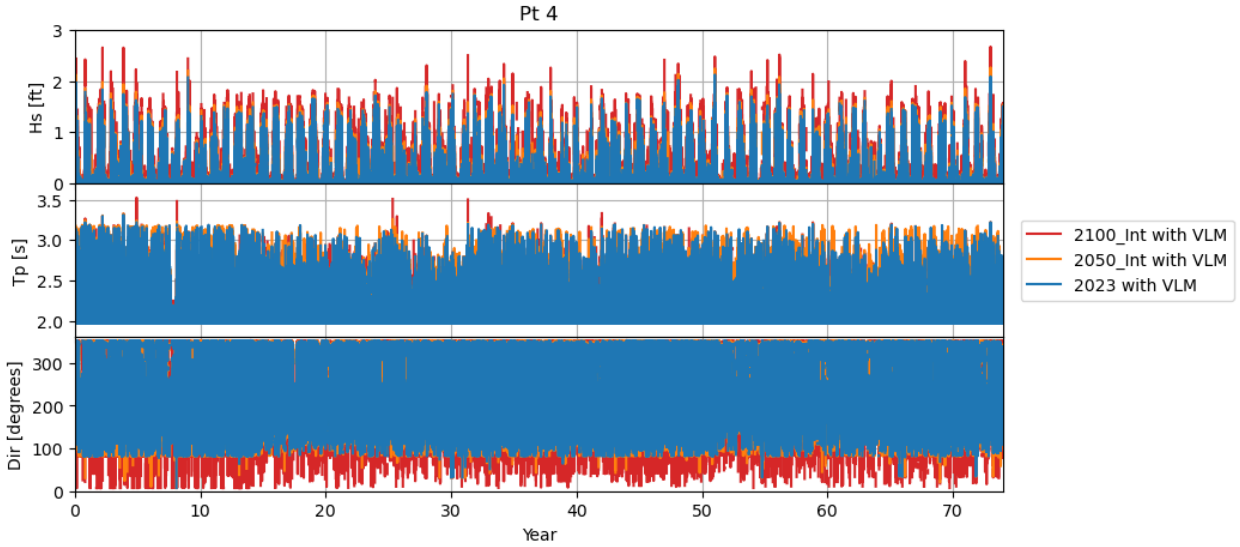

Figure 5.2.1: [Top] Significant wave time series [Middle] Peak wave period and [Bottom] Peak wave direction at Point 4 created from LUT (Figures 5.1.3-4) using the historical storm record (Figures 4.1.4-5) and reference water levels at various sea level futures (Figure 4.3.1).

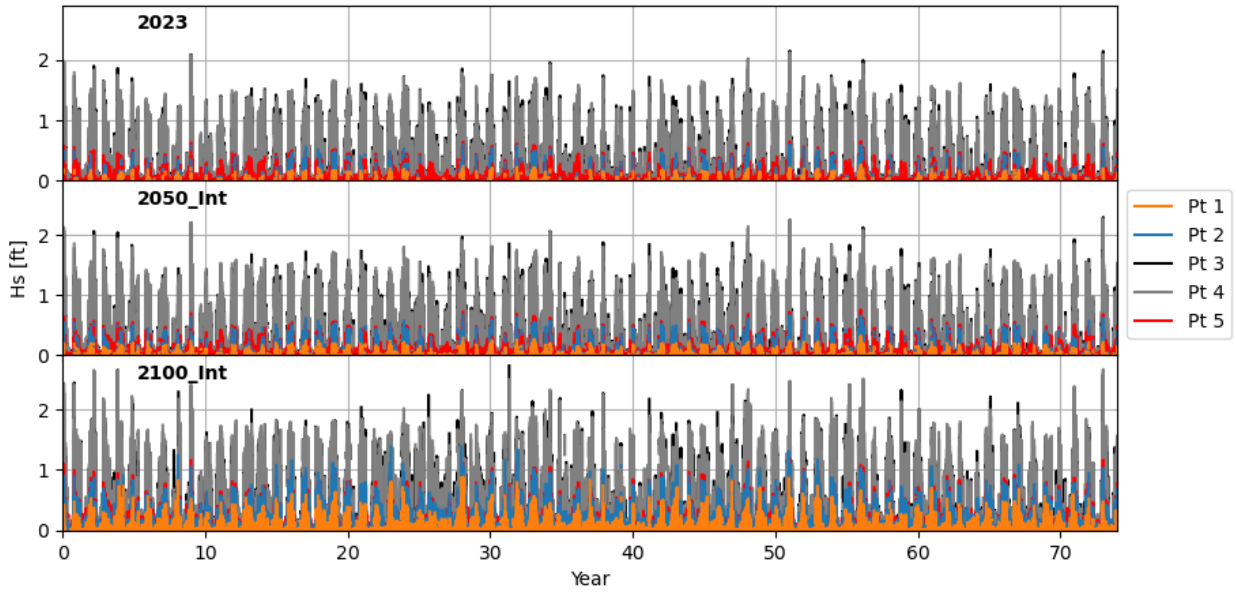

Figure 5.2.2: Significant wave height time series at each point created from LUT (Figures 5.1.3-4) using the historical storm record (Figures 4.1.4-5) and reference water levels at various sea level

futures (Figure 4.3.1). [Top] 2023 [Middle] 2050 Intermediate SLR future [Bottom] 2100 Intermediate SLR future.

6. Wave runup and coastal discharge: EurOTop formulations

The $R_{2\%}$ wave runup elevations, overtopping discharge and overflow discharge were estimated for each extraction point and SLR future following the EuroTop (2018) methods, using the shoreline characteristics listed in Table 1.4.2 and the bulk wave time series. The EurOTop equations are consistent with the Technical Advisory Committee for Water Retaining Structures (TAW) method (van der Meer 2002) typically used by FEMA (2005 and 2014), just with more up-to-date parameters.

The "Iribarren", or "surf similarity" parameter, $\xi_{m-1,0}$ is used throughout the EurOTop equations which relates the shoreline structure steepness to the wave steepness $s_{m-1,0} = H_s/L_{m-1,0}$,

$$\xi_{m-1,0} = \frac{m}{\sqrt{\frac{Hs}{L_{m-1,0}}}} \qquad \textit{Equation 6.1}$$

where

$$L_{m-1,0} = \frac{gT_{m-1,0}^2}{2\pi} \qquad \textit{Equation 6.2}$$

and

$$T_{m-1,0} = \frac{T_p}{1.1} \qquad \textit{Equation 6.3}$$

where m is the slope of the structure, H_s is significant wave height, T_p is peak wave period, and g is acceleration due to gravity 9.81 m/s^2. Wave height and period are modified for very oblique waves, $80^\circ < |\beta| \leq 110^\circ$, due to diffraction around the structure:

H_s multiplied by $\frac{110 - |\beta|}{30}$ *Equation 6.4*

$T_{m-1,0}$ multiplied by $\sqrt{\frac{110 - |\beta|}{30}}$ *Equation 6.5*

where β is the wave attack angle, which is the wave direction relative to the structure orientation (Figure 6.1).

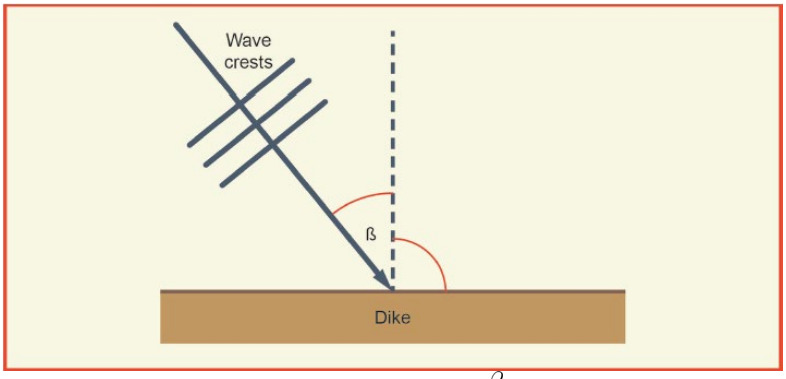

Figure 6.1: Definition of angle of wave attack β. Figure from EurOTop (2018).

6.1 Wave runup

Wave runup, $R_{2\%}$ generally follows this formula,

$$R_{2\%} = 1.75 H_s \gamma_b \gamma_f \gamma_\beta \xi_{m-1,0}, \qquad \textit{Equation 6.1.1}$$

but cannot exceed this maximum:

$$R_{2\%} = 1.07 H_s \gamma_{f\ surging} \gamma_\beta (4.3 - \frac{1.5}{\sqrt{\gamma_b \xi_{m-1,0}}}), \qquad \textit{Equation 6.1.2}$$

or this maximum:

$R_{2\%} = 3.21 H_s$ (impermeable core) *Equation 6.1.3*

where some of the parameters depend on the shoreline structure type (ORP = Old Rail Prism, RSP = Rocky Shore Protection, Table 1.4.2):

Influence factor for a berm: *Equation 6.1.4*

$\gamma_b = 1$

Influence factor for friction: *Equation 6.1.5*

$\gamma_f = 0.9$ for ORP

$\gamma_f = 0.55$ for RSP

Influence factor for surging waves in a rubble mound structure: *Equation 6.1.6*

$\gamma_{f\ surging} = \gamma_f$ for ORP

$\gamma_{f\ surging} = \gamma_f$ for RSP when $\xi_{m-1,0} < 1.8$

$\gamma_{f\ surging} = \gamma_f + (\xi_{m-1,0} - 1.8)(1 - \gamma_f)/8.2$ for RSP when $\xi_{m-1,0} > 1.8$

Influence factor for oblique waves: *Equation 6.1.7*

$\gamma_\beta = 1 - 0.0022|\beta|$ for $0° \leq \beta \leq 80°$ for ORP
$\gamma_\beta = 0.824$ for $\beta > 80°$ for ORP
$\gamma_\beta = 1 - 0.0063|\beta|$ for $0° \leq \beta \leq 80°$ for RSP
$\gamma_\beta = 1 - 0.0063|80°|$ for $\beta > 80°$ for RSP

If the waves are extremely oblique, there is no runup:

$R_{2\%} = 0$ for $\beta > 110°$. *Equation 6.1.8*

Note that points 3 and 4 generally experience the largest modeled runup (max of around 4ft by the 2050 Intermediate SLR future), which is primarily due to the absence of salt marsh fronting these sites (Figure 6.1.1)**. In contrast, max modeled runup at points 1, 2, and 5 is approximately 2 feet or less by the 2050 Intermediate future.**

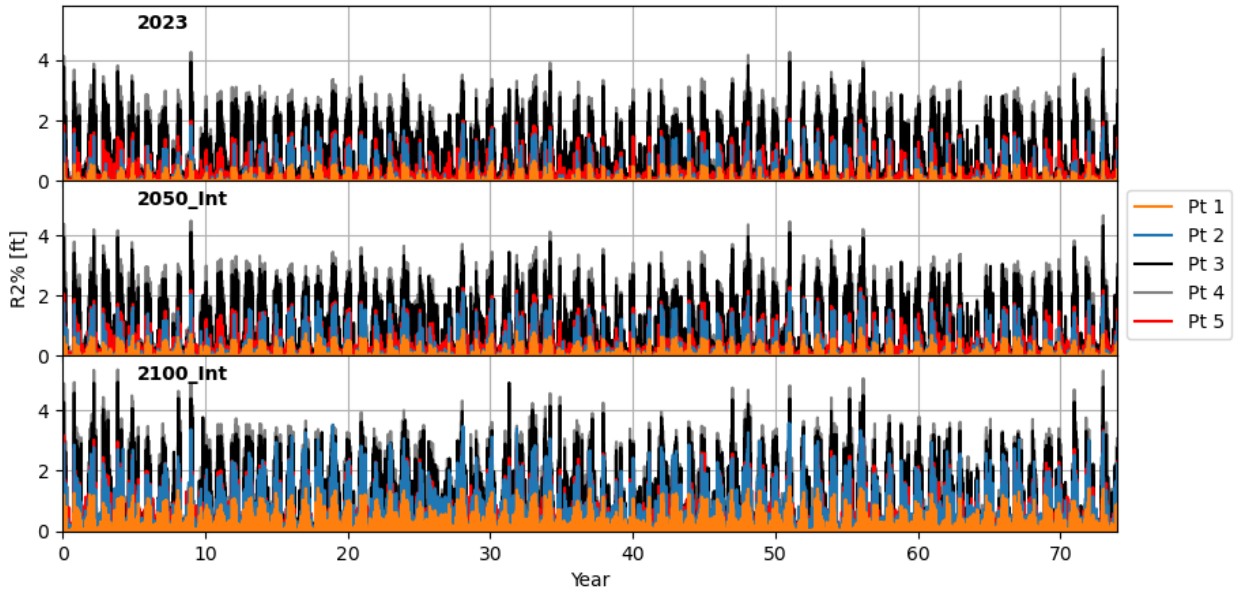

Figure 6.1.1: $R_{2\%}$ time series estimated using EurOTop (2018), the modeled wave conditions (Figures 5.2.1-2), and shoreline structure characteristics (Table 1.4.2). [Top] 2023. [Middle] 2050 Intermediate SLR future. [Bottom] 2100 Intermediate SLR future.

6.2 Coastal discharge

Coastal discharge can be caused by wave runup overtopping the crest, $q_{overtop}$, or from reference water level (RWL) exceeding the crest height $q_{overflow}$. Overflow occurs when the crest freeboard, $R_c = structure\ crest\ height - RWL$, is negative:

$$q_{overflow} = 0.54\sqrt{g|-R_c^3|} \quad \textit{Equation 6.2.1}$$

Overtopping discharge generally follows this formula (where R_c is set to zero for negative freeboard):

$$q_{overtop} = 0.026 C_r \sqrt{\frac{gH_s^3}{m}} \gamma_b \xi_{m-1,0} exp[-(2.5 \frac{R_c}{\xi_{m-1,0} H_s \gamma_b \gamma_f \gamma_{beta} \gamma_v})^{1.3}] \quad \textit{Equation 6.2.2}$$

but cannot exceed this maximum:

$$q_{overtop} = 0.1035 C_r \sqrt{gH_s^3} exp[-(1.35 \frac{R_c}{H_s \gamma_f \gamma_{beta} \gamma_*})^{1.3}] \quad \textit{Equation 6.2.3}$$

where some of the parameters depend on the shoreline structure type (ORP = Old Rail Prism, RSP = Rocky Shore Protection, Table 1.4.2):

Influence factor for berm: *Equation 6.2.4*

$\gamma_b = 1$

Influence factor for wall on a slope:

$\gamma_v = 1$

Combined influence factor for a storm wall on a slope or promenade:

$\gamma_* = 1$

Influence factor for friction *Equation 6.2.5*

$\gamma_f = 0.9$ for ORP

$\gamma_f = 0.55$ for RSP

Influence factor for surging waves in a rubble mound structure: *Equation 6.2.6*

$\gamma_{f\ surging} = \gamma_f$ for ORP

$\gamma_{f\ surging} = \gamma_f$ for RSP when $\xi_{m-1,0} < 5$

$\gamma_{f\ surging} = \gamma_f + (\xi_{m-1,0} - 5)(1 - \gamma_f)/5.0$ for RSP when $\xi_{m-1,0} > 5$

Influence factor for oblique waves: *Equation 6.2.7*

$\gamma_\beta = 1 - 0.0033|\beta|$ for $0^\circ \leq \beta \leq 80^\circ$ for ORP

$\gamma_\beta = 0.736$ for $\beta > 80^\circ$ for ORP

$\gamma_\beta = 1 - 0.0063|\beta|$ for $0^\circ \leq \beta \leq 80^\circ$ for RSP

$\gamma_\beta = 1 - 0.0063|80^\circ|$ for $\beta > 80^\circ$ for RSP

Armoured crest reduction factor: *Equation 6.2.8*

$C_r = 1$ for ORP

$C_r = 3.06 exp(-1.5 G_c / H_s)$ with max $C_r = 1$ for RSP

where G_c is the structure crest width.

If the waves are extremely oblique, there is no overtopping discharge:

$q_{overtop} = 0$ for $\beta > 110^\circ$. *Equation 6.2.9*

The total coastal discharge is the sum of the overtopping and overflow discharge:

$$q_{total} = q_{overflow} + q_{overtop} \quad \textit{Equation 6.2.10}$$

Before reference water levels become elevated above the structure crest, overtopping occurs when runup washes over the crest. These volumetric overtopping flow rates per meter shoreline are much smaller than the overflow discharges that occur when there is no remaining freeboard (when reference water levels exceed the structure crest height). The total discharge is the sum of the overtopping and overflow discharge (which is dominated by overflow). Estimates of these discharge quantities are shown for each extraction point in Figures 6.2.1-5. **Modeled coastal discharge is only shown for the 2023 and 2050 Intermediate futures because overflow discharges become large at all locations farther into the future due to RWLs exceeding structure crest heights (Section 4.3). During the 2023 and 2050 Intermediate SLR futures, overtopping and overflow occurs most frequently at Points 2 and 5 because these locations have the lowest structure crest height. *Discharge only constitutes flooding if it overwhelms drainage capabilities.*** Note the difference in the y-axis scales of the overtopping and overflow discharges.

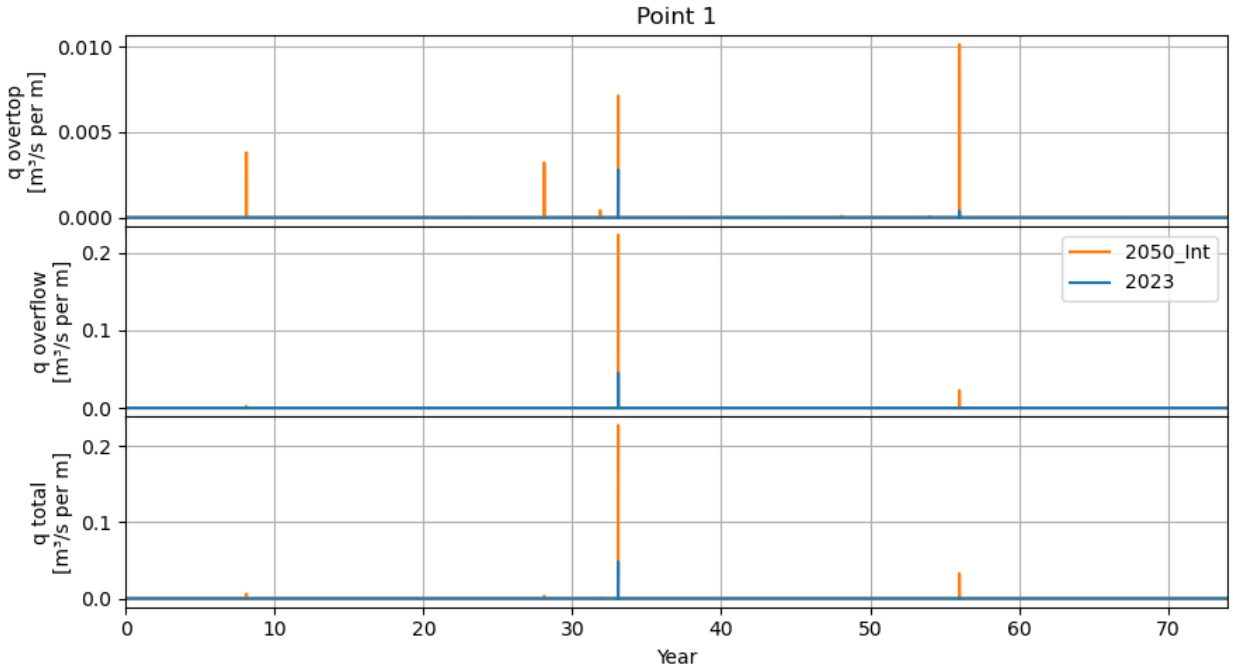

Figure 6.2.1 Time series of discharge quantities at Point 1 for 2023 and future 2050 Intermediate SLR using the historical storm record.

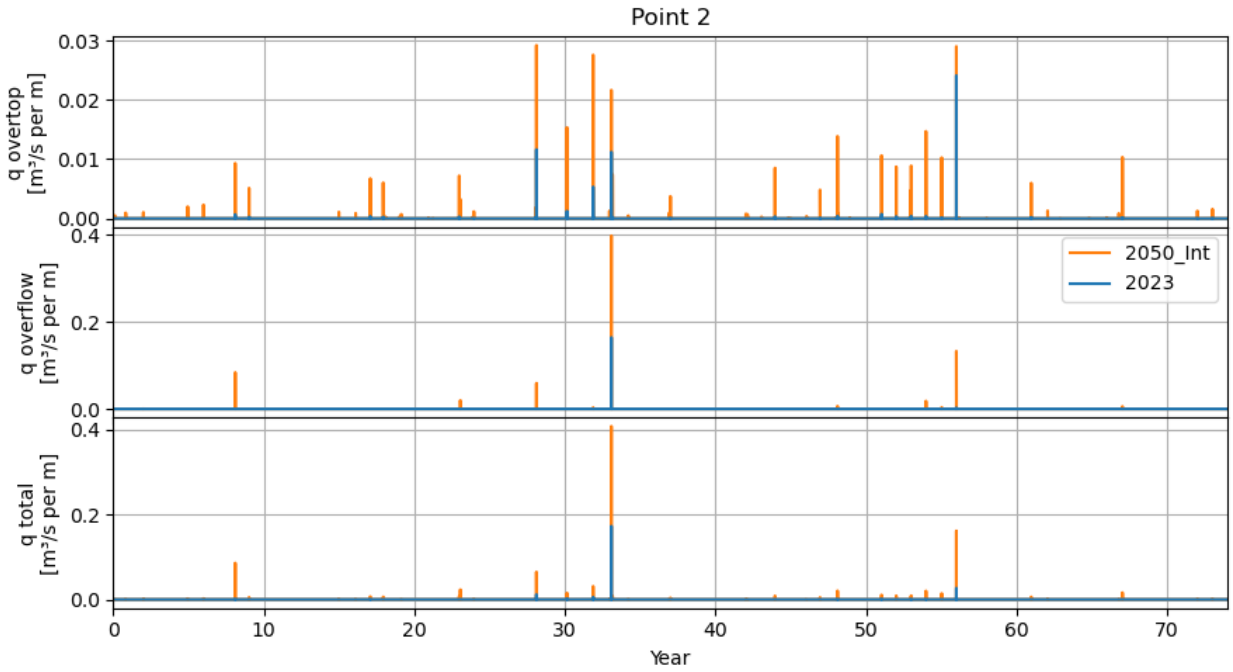

Figure 6.2.2 Time series of discharge quantities at Point 2 for 2023 and future (2050 Intermediate) SLR based on historical storm record.

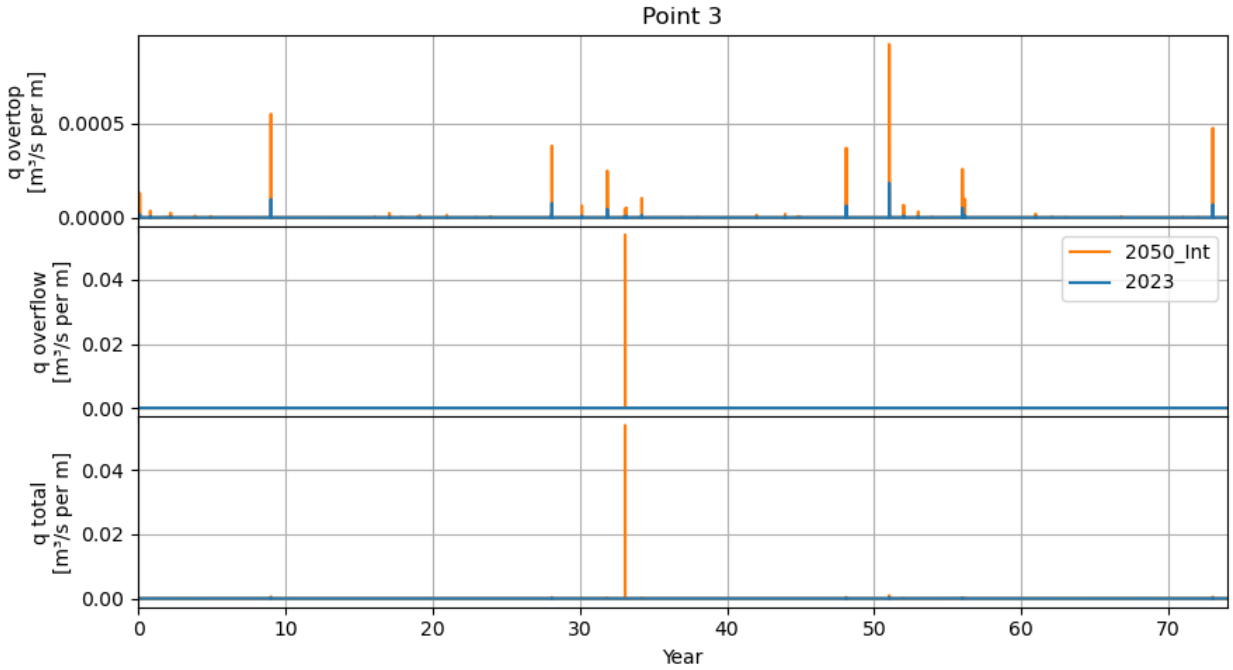

Figure 6.2.3 Time series of discharge quantities at Point 3 for 2023 and future 2050 Intermediate SLR using the historical storm record.

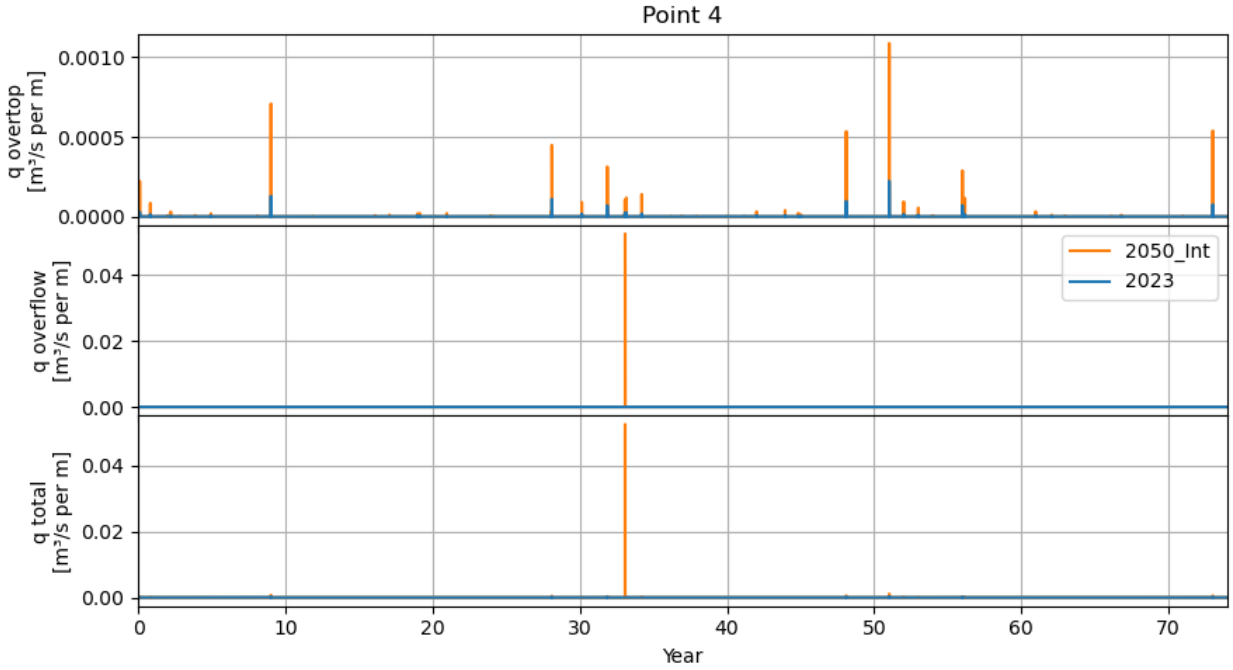

Figure 6.2.4 Time series of discharge quantities at Point 4 for 2023 and future 2050 Intermediate SLR using the historical storm record.

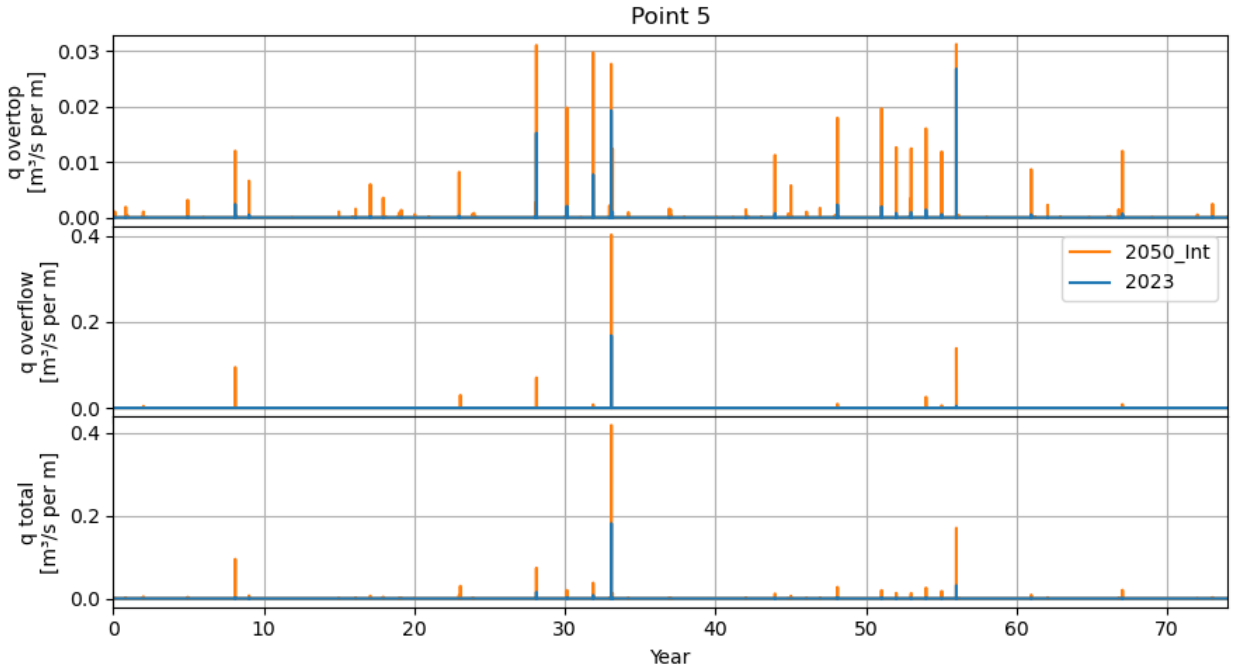

Figure 6.2.5 Time series of discharge quantities at Point 5 for 2023 and future 2050 Intermediate SLR using the historical storm record.

7. Historical water levels and the 2005 NYE storm

The only recorded flooding event along the Eureka/Arcata corridor happened on New Years Eve (NYE) Dec 31, 2005 during a high tide and high wind event (Figure 7.1). The flooding occurred near extraction points 3 and 4 (Figure 1.4.1).

Figure 7.1 [Top] Eureka/Arcata corridor flooding and [Bottom] Spindrift from strong winds during the 2005 New Years Eve storm.

To assess whether we captured this event, we recreated the historical water level time series. First we added the observed trend from the North Spit tide gauge into the EFDC modeled reference water levels. Then we used those reference levels and the observed winds to generate wave time series at each extraction point using the LUTs (Figure 7.2 and 7.3). While the 2005 NYE event looks like a max extreme in Figure 7.2, when we zoom in using Figure 7.3, it appears the storm the day before is actually causing higher total water levels in our model. It seems that we are not capturing the 2005 NYE wind event properly (Figure 7.4). **The National Weather Service at Woodley Island recorded a max wind gust on 2005 NYE of 56 knots. Converting to mps, then using Equation 4.1.3 to convert a 3-sec gust to a 1-hour sustained wind speed, and multiplying**

by a factor of 1.2 to adjust from land to over-water winds gives 23 mps, suggesting we are underestimating this wind event.

Note that points 3 and 4 generally experience the largest runup, which is largely due to the absence of salt marsh fronting these sites. Additionally, we see that total water levels are sometimes exceeding the crest height threshold. However, due to the set back nature of the highway relative to the shoreline protection structures and the drainage ditches between them (Figure 1.4.7)**, overtopping of the structure does not necessarily constitute flooding of the highway.**

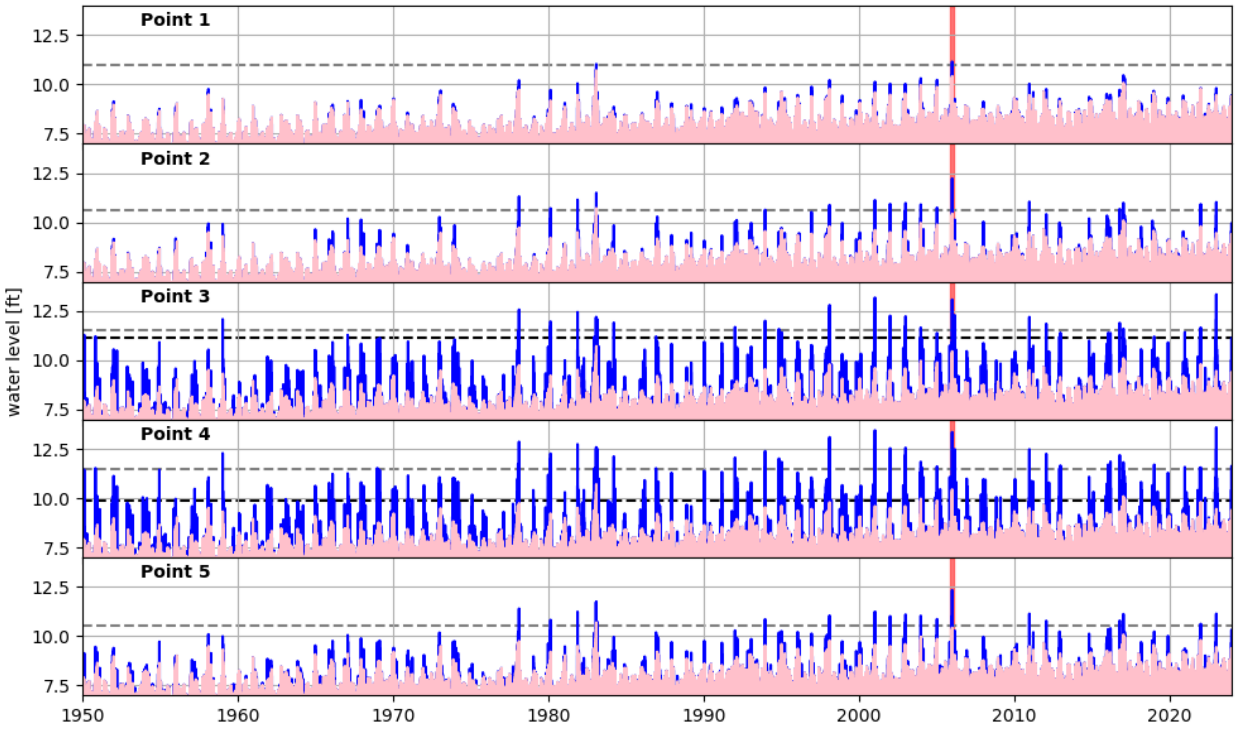

Figure 7.2: Historical total water levels (blue) and reference water levels (pink) at each extraction point. The NYE 2005 storm is shown as a red vertical line. The structure crest height given in Table 1.4.2 is shown as a gray horizontal dashed line, which incorrectly assumes that Points 3 and 4 had been elevated due to Bay Trail construction. A black horizontal line at the crest height in the 2020 CoNED TBDEM represents the historical condition at Points 3 and 4.

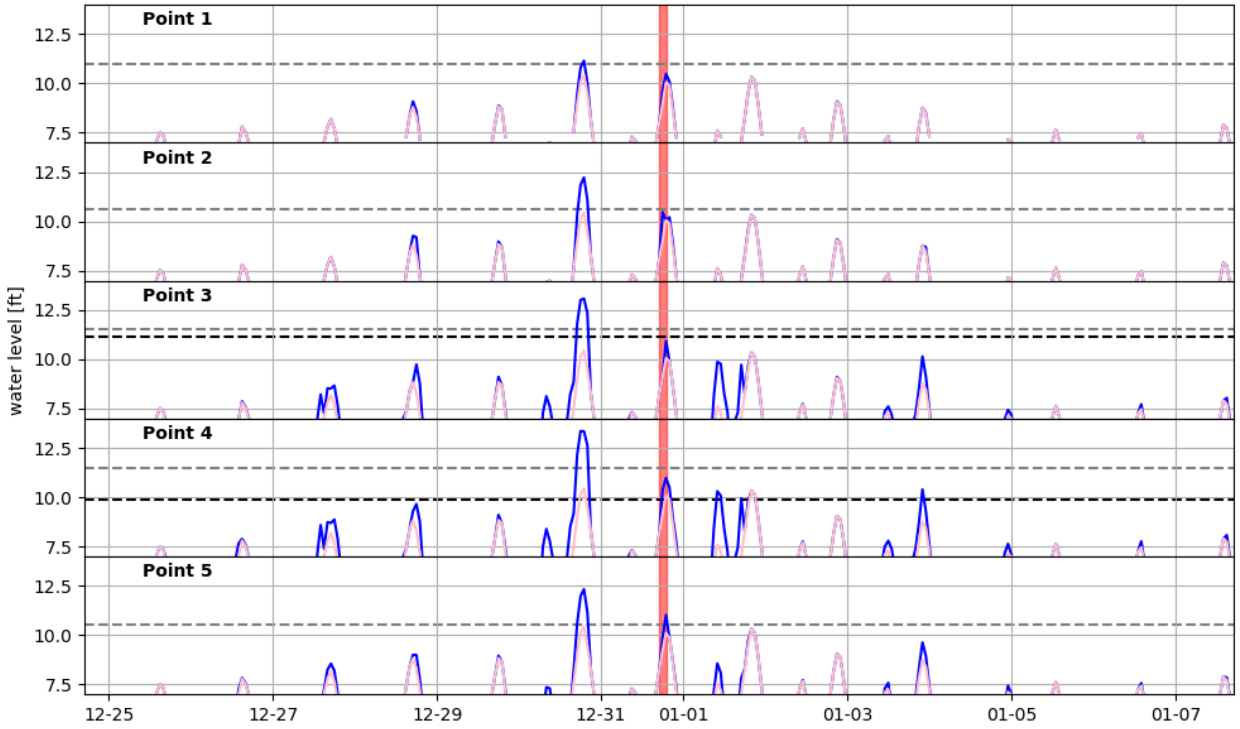

Figure 7.3: Same as Figure 7.2 but zoomed in on the 2005 NYE storm (red vertical bar). The storm event the day prior was actually larger at all locations.

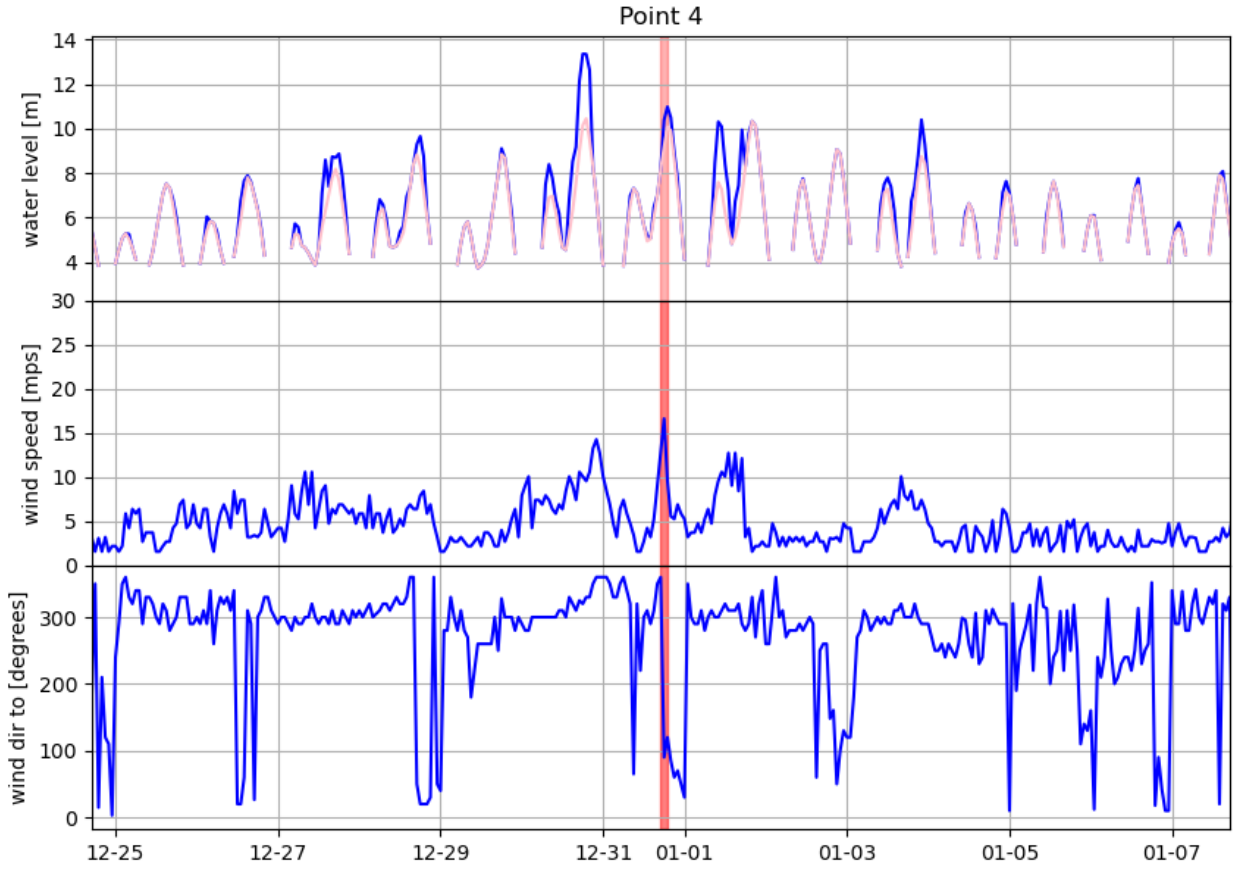

Figure 7.4: 2005 NYE Storm [Top]: Same as 7..3 but for Point 4 only. [Middle]: Wind speed time series. [Bottom] Time series of the cartesian direction the wind is blowing towards.

8. Main points and Recommendations

- Levees, drainage structures, railroad prisms and the Eureka/Arcata Highway prism have blocked tidewaters, reduced salt marsh, and modified the shoreline. **The new Bay Trail will further alter the shoreline, where Points 3 and 4 will have the tallest protective shoreline structure crest height. However, the highway elevation is lowest at Points 3 and 4, so these locations could still be the most vulnerable if water gets in elsewhere.**
    - Recommendation: Collect lidar survey data post Bay Trail construction to accurately map new shoreline configuration.

- Points 1, 2, and 5 are fronted by salt marsh, while Points 3 and 4 are mostly fronted by mudflats due to salt marsh erosion.

  - Recommendation: Collect lidar survey data seasonally, for multiple years, to understand the evolution of sediment levels and vegetation coverage fronting the project shoreline at each location.

- The amount of future sea level rise (SLR) depends on emissions and the climate's physical response. The Low scenario represents the lower edge of plausibility and aggressive emissions reductions. The Intermediate-Low scenario is the lower bound of the most likely SLR, while the Intermediate is the upper bound of the most likely SLR. The Intermediate-High scenario is associated with high emissions and low confidence ice processes, while the High scenario requires very high emissions and lots of low confidence ice processes. Additionally, vertical land motion (VLM) contributes to *relative* sea level rise. From available data, it is unclear whether locations along the corridor are uplifting or subsiding. As a conservative approach, we use the Mad River Slough tide gauge's subsiding VLM rate (-0.54mm) for all sites along the corridor.
  - Recommendation: Install a tide gauge along the corridor shoreline to continuously monitor SLR and VLM.

- Modeled max reference water levels are elevated above the entrance bay still water levels due to tidal amplification (~0.5 ft) and wind setup (~2 ft). **Results show that by the 2100 Intermediate SLR future, modeled RWLs are regularly above the crest height elevations at all locations, suggesting the existing highway will be regularly flooded at this SLR future.**
  - Recommendation: Install an anemometer on one of the small sand islands in the middle of North Bay and monitor winds for a couple of years to better understand local winds directly over the bay and their contribution to wind setup.

- As seas rise, wave heights increase due to reduced depth-limited wave breaking. By the 2050 Intermediate SLR future ~2 ft max modeled wave heights occur at Points 3 and 4, while max modeled waves are only ~0.5ft at Points 1, 2, and 5 due to the protection provided by the salt marsh.
  - Recommendation: Install an array of wave resolving pressure sensors (and/or an acoustic doppler current profiler with wave measuring capabilities) for a couple of years (ideally with the same deployment time period as the anemometer and spanning the seasonal lidar surveys) in eastern Arcata Bay to measure waves and calibrate the wave model.

- Water levels at the shoreline are further elevated by wave runup. By the 2050 Intermediate SLR future, the largest modeled runup is about ~4ft at Points 3 and 4, due to the absence of salt marsh fronting these sites. In contrast, max modeled runup at points 1, 2, and 5 is approximately 2 feet or less by the 2050 Intermediate future.

- Recommendation: Install a pressure sensor inside the shoreline protection structure at each location for a couple of years (ideally with the same deployment time period as the anemometer and wave sensors and spanning the seasonal lidar surveys) to calibrate the runup estimations.

- Modeled coastal discharge is only shown for the 2023 and 2050 Intermediate futures because overflow discharges become large at all locations farther into the future due to RWLs exceeding structure crest heights (Section 4.3). **During the 2023 and 2050 Intermediate SLR futures, overtopping and overflow occurs most frequently at Points 2 and 5 because these locations have the lowest structure crest height. *Discharge only constitutes flooding if it overwhelms drainage capabilities.***
  - Recommendation: A comparison of these modeled discharge estimates with modeled drainage capabilities will be analyzed in a future memo, in collaboration with the Riverine Hazards working group.

- Modeled total water level results do not identify the only known coastal flooding event as extreme. A comparison of the wind forcing data in our model to local wind gust measurements (converted to an hourly over-water wind speed) suggest that we are underestimating the intensity (and perhaps misjudging the direction) of the wind during this event.
  - Recommendation: An update will be provided in a future memo after improving the wind estimates using additional wind data sources.

References

Arns, A., T. Wahl, I.D. Haigh, J. Jensen, and C. Pattiaratchi. (2013). Estimating extreme water level probabilities: A comparison of the direct methods and recommendations for best practice. Coastal Engineering, Volume 81, 51-66.

Barnhart, R. A., M. J. Boyd., and J. E. Pequegnat. 1992. The ecology of Humboldt Bay, California: an estuarine profile (Vol. 1). U.S. Department of the Interior, Fish and Wildlife Service, Washington, District of Columbia, USA.

Battjes, J.A., Janssen, J.P.F.M., 1978. Energy loss and set-up due to breaking of random waves. In: Proceedings of the 16th International Conference on Coastal Engineering. ASCE, pp. 569–587.

Booij, N., Ris, R.C., Holthuijsen, L.H., 1999. A third-generation wave model for coastal regions, Part I, Model description and validation. J. Geophys. Res. Oceans 104, 7649–7666.

Booij, N., L.H. Holthuijsen and M.P. Benit, 2009: A distributed collinear triad approximation in SWAN, Coastal Dynamics 2009, pp. 1-10.

Brown, L., 2019. California Salt Marsh Accretion, Ecosystem Services, and Disturbance Responses In the Face of Climate Change. Doctoral dissertation, UCLA, 239 p.

California Trout, Stillwater Sciences, and Northern Hydrology & Engineering. 2019. Elk River Recovery Assessment: Recovery Framework. Prepared by California Trout, Arcata, CA; Stillwater Sciences, Arcata, CA; and Northern Hydrology & Engineering, McKinleyville, CA for North Coast Regional Water Quality Control Board, Santa Rosa, CA.

California Sea Level Rise Guidance: 2024 Science and Policy Update. 2024. California Sea Level Rise Science Task Force, California Ocean Protection Council, California Ocean Science Trust.

Coastal Engineering Manual (CEM). 2015. Chapter 2, Meteorology and Wave Climate. U.S. Army Corps of Engineers. Washington D.C. EM 1110-2-1100 (Part II).

County of Humboldt Department of Public Works (CHDPW), 2022. Project plans for construction of Humboldt Bay Trail South. PROJECT NO. RPSTPL-5904(143), RPL-5904(180), AND ATPL-5904(182) CONTRACT NO. 715036.

Coles, S. 2001. An introduction to statistical modeling of extreme values. Springer-Verlag, London.

Collins, J. I. (1972). Prediction of shallow-water spectra. Journal of Geophysical Research, 77(15), 2693-2707.

Costa and Glatzel. 2002. Steven L. Costa and Karen A. Glatzel, Humboldt Bay, California, Entrance Channel Report 1: Data Review, Prepared for U.S. Army Corps of Engineers, Engineering Research and Development Center

Crosby, S. C., Nederhoff, C. M., VanArendonk, N., & Grossman, E. E. (2023). Efficient modeling of wave generation and propagation in a semi-enclosed estuary. Ocean Modelling, 184, 102231.

Curtis, J. A., C. Freeman, and K. Thorne. 2019 Early results-salt marsh response to changing fine-sediment supply conditions, Humboldt Bay, CA.

Curtis, J. A., Flint, L. E., Stern, M. A., Lewis, J., & Klein, R. D. (2021). Amplified impact of climate change on fine-sediment delivery to a subsiding coast, Humboldt Bay, California. Estuaries and Coasts, 44(8), 2173-2193.

Dalrymple, R.A., J.T. Kirby and P.A. Hwang, 1984: Wave diffraction due to areas of energy dissipation, Journal of Waterways, Ports, Harbours and Coastal Engineering, 110, 67-79.

DSI LLC. 2023. EFDC+ Theory, Version 11.8. Published by DSI LLC, Edmonds, WA. Available at: https://www.eemodelingsystem.com/wp-content/Download/Documentation/EFDC_Theory_Document_Ver_11.pdf.

Environmental Science Associates (ESA). 2018. Sea level Rise Vulnerability and Adaptation Report, Humboldt Bay Trail South. Report Prepared by ESA for County of Humboldt, Under Contract with GHD, June 2018.

EurOtop, 2018. Manual on wave overtopping of sea defenses and related structures. An overtopping manual largely based on European research, but for worldwide application. Van der Meer, J.W., Allsop, N.W.H., Bruce, T., De Rouck, J., Kortenhaus, A., Pullen, T., Schüttrumpf, H., Troch, P. and Zanuttigh, B., www.overtopping-manual.com.

Federal Emergency Management Agency (FEMA), 2005. Final Draft Guidelines for Coastal Flood Hazard Analysis and Mapping for the Pacific Coast of the United States. Joint Project by FEMA Region IX, FEMA Region X, and FEMA Headquarters. FEMA Region IX, Oakland, CA.

Federal Emergency Management Agency (FEMA), 2014. Intermediate Data Submittal #3: Nearshore Hydraulics, Humboldt County, California. Prepared for FEMA Region IX. Prepared by Baker AECOM.

George, D.A. and P.S. Hill. 2008. Wave climate, sediment supply and the depth of the sand-mud transition: A global survey. Marine Geology 254, 121-128.

GHD. 2018. City of Eureka Storm Water Resources Plan.

GHD Inc., 2021. Sea Level Rise Adaptation Plan for Transportation Infrastructure and Other Critical Resources in the Eureka Slough Hydrographic Area, Humboldt Bay. Prepared for Humboldt County Department of Public Works, Humboldt County Association of Governments, City of Eureka, and Caltrans District 1. Project Team: Environmental Science Associates (ESA), GHD, Northern Hydrology & Engineering (NHE), Philip King and Kristina Kunkel (San Francisco State University), Redwood Community Action Agency (RCAA), Trinity Associates

GHD Inc., Northern Hydrology & Engineering, and Conor Shea. 2022. Natural Shoreline Infrastructure in Humboldt Bay for Intertidal Coastal Marsh Restoration and Transportation Corridor Protection: Draft 50% Design Report. Prepared for Humboldt County Department of Public Works. Draft report and appendices available at https://humboldtgov.org/2487/Sea-Level-Rise.

Griggs, G, Árvai, J, Cayan, D, DeConto, R, Fox, J, Fricker, HA, Kopp, RE, Tebaldi, C, Whiteman, EA (California Ocean Protection Council Science Advisory Team Working Group). Rising Seas in California: An Update on Sea-Level Rise Science. California Ocean Science Trust, April 2017.

Hamrick, J. M. 1992. A Three-Dimensional Environmental Fluid Dynamics Computer Code: Theoretical and Computational Aspects. The College of William and Mary, Virginia Institute of Marine Science, Special Report 317.

Hasselmann, K., et al., 1973. Measurements of Wind-Wave Growth and Swell Decay during the Joint North Sea Wave Project (JONSWAP). Deutches Hydrographisches Institute.

Hasselmann, S., Hasselmann, K., Allender, J.H., Barnett, T.P., 1985. Computations and parameterizations of the nonlinear energy transfer in a gravity-wave spectrum. Part II. Parameterizations of the Nonlinear Energy Transfer for Application in Wave Models 15, 78–1391.

Holthuijsen, L.H., 2007: Waves in oceanic and coastal waters, Cambridge University Press.

Kahma, K. K., & Calkoen, C. J. (1992). Reconciling discrepancies in the observed growth of wind-generated waves. Journal of Physical Oceanography, 22(12), 1389-1405.

Komen, G.J., Hasselmann, S., Hasselmann, K., 1984. On the existence of a fully developed wind-sea spectrum. J. Phys. Oceanogr. 14, 1271–1285.

Laird, A., Powell, B. and J.K. Anderson. 2013. Humboldt Bay Shoreline Inventory, Mapping and Sea level Rise Vulnerability Assessment. Humboldt Bay Sea Level Rise Adaptation Planning Project, Phase 1. Prepared for the California State Coastal Conservancy.

Mariotti, G., & Fagherazzi, S. (2013). Wind waves on a mudflat: The influence of fetch and depth on bed shear stresses. Continental Shelf Research, 60, S99-S110.

Masson-Delmotte, V., P. Zhai, A. Pirani, S.L. Connors, C. Péan, S. Berger, N. Caud, Y. Chen, L. Goldfarb, M.I. Gomis, M. Huang, K. Leitzell, E. Lonnoy, J.B.R. Matthews, T.K. Maycock, T. Waterfield, O. Yelekçi, R. Yu, & B. Zhou (Eds.). (2021). Climate Change 2021: The Physical Science Basis. Contribution of Working Group I to the Sixth Assessment Report of the Intergovernmental Panel on Climate Change. Cambridge University Press. https://www.ipcc.ch/report/ar6/wg1/

Northern Hydrology & Engineering (NHE). 2015. Humboldt Bay: Sea Level Rise, Hydrodynamic Modeling, and Inundation Vulnerability Mapping. Prepared for the State Coastal Conservancy, and Coastal Ecosystems Institute of Northern California. McKinleyville, CA.

OCM Partners. 2024. 1986 -2019 USGS CoNED Topobathy DEM (Compiled 2020): Northern California. Available at: https://www.fisheries.noaa.gov/inport/item/62987.

Patton, J. R., Williams, T.B., Anderson, J.A., Hemphill-Haley, M., Burgette, R.J., Weldon, R. II, McPherson, R.C., and T.H. Leroy. 2023a. 20th to 21st Century Relative Sea and Land Level Changes in Northern California: Tectonic Land Level Changes and their Contribution to Sea-Level Rise, Humboldt Bay Region, Northern California in Tektonika, v. 1, no. 1, https://doi.org/10.55575/tektonika2023.1.1.6.

Patton, J. R., Williams, T.B., Anderson, J.A., Hemphill-Haley, M., Burgette, R.J., Weldon, R. II, McPherson, R.C., and T.H. Leroy. 2023b. Zenodo Repository for: 20th to 21st Century Relative Sea and Land Level Changes in Northern California: Tectonic Land Level Changes and their Contribution to Sea-Level Rise, Humboldt Bay Region, Northern California in Tektonika, v. 1, no. 1, https://doi.org/10.5281/zenodo.7420440.

Pierson Jr, W. J., & Moskowitz, L. (1964). A proposed spectral form for fully developed wind seas based on the similarity theory of SA Kitaigorodskii. Journal of geophysical research, 69(24), 5181-5190.

Pintar, A.L., Simiu, E., Lombardo, F.T. and M. Levitan. 2015. Maps of Non-Hurricane Non-tornadic Wind Speeds With Specified Mean Recurrence Intervals for the Contiguous United States Using a Two-Dimensional Poisson Process Extreme Value Model and Local Regression. National Institute of Standards and Technology (NIST) Special Publication 500-301.

Richmond, L., Anderson, J., Archibald, J., Brown, A., Canter, A., Cashman, E., ... & Wilkinson, H. (2023). Transformative Sea-Level Rise Research and Planning. Humboldt Journal of Social Relations, 45, 67-93.

Rohde, J.. June 2020. Humboldt Bay Shoreline, North Eureka to South Arcata: A History of Cultural Influences.

Suzuki, T., M. Zijlema, B. Burger, M. C. Meijer, and S. Narayan, 2012: Wave dissipation by vegetation with layer schematization in SWAN, Coastal Engineering, 59(1), 64-71.

SWAN Team, 2024. SWAN User Manual, SWAN Cycle III Version 41.45AB. Delft University of Technology, Netherlands, p. 154 available online from: http://www.swan.tudelft.nl.

Sweet, W.V., B.D. Hamlington, R.E. Kopp, C.P. Weaver, P.L. Barnard, D. Bekaert, W. Brooks, M. Craghan, G. Dusek, T. Frederikse, G. Garner, A.S. Genz, J.P. Krasting, E. Larour, D. Marcy, J.J. Marra, J. Obeysekera, M. Osler, M. Pendleton, D. Roman, L. Schmied, W. Veatch, K.D. White, and C. Zuzak, 2022: Global and Regional Sea Level Rise Scenarios for the United States: Updated Mean

Projections and Extreme Water Level Probabilities Along U.S. Coastlines. NOAA Technical Report NOS 01. National Oceanic and Atmospheric Administration, National Ocean Service, Silver Spring, MD, 111 pp. https://oceanservice.noaa.gov/hazards/sealevelrise/noaa-nos-techrpt01-global-regional-SLR-scenarios-US.pdf

Thompson, R.W., 1971, Recent Sediments of Humboldt Bay, Eureka, California, Final Report, Petrol Reserve Fund, PRF #789-G2, 46 pp.

U.S. Army Corps of Engineers (USACE). 2017 Eureka Littoral Cell Coastal Regional Sediment Management Plan

van der Meer, J.W. (2002). Technical Report: Wave Run-up and Overtopping at Dikes. Technical Advisory Committee for Water Retaining Structures, Delft, Netherlands.

Wheatcroft, R.A. and J.C. Borgeld. 2000. Oceanic flood deposits on the northern California shelf: large-scale distribution and small-scale physical properties. Continental Shelf Research 20, p. 2163–2190.

Whitham, G.B., 1974: Linear and nonlinear waves, Wiley, New York

Wiyot Tribe, 2024: History. Wiyot Tribe. https://www.wiyot.us/148/Cultural